



HAL
open science

Susceptibility of planetary atmospheres to mass loss and growth by planetesimal impacts: the impact shoreline

M Wyatt, Q Kral, C Sinclair

► **To cite this version:**

M Wyatt, Q Kral, C Sinclair. Susceptibility of planetary atmospheres to mass loss and growth by planetesimal impacts: the impact shoreline. *Monthly Notices of the Royal Astronomical Society*, 2020, 491 (1), pp.782-802. 10.1093/mnras/stz3052 . hal-03259643

HAL Id: hal-03259643

<https://hal.science/hal-03259643>

Submitted on 24 May 2024

HAL is a multi-disciplinary open access archive for the deposit and dissemination of scientific research documents, whether they are published or not. The documents may come from teaching and research institutions in France or abroad, or from public or private research centers.

L'archive ouverte pluridisciplinaire **HAL**, est destinée au dépôt et à la diffusion de documents scientifiques de niveau recherche, publiés ou non, émanant des établissements d'enseignement et de recherche français ou étrangers, des laboratoires publics ou privés.

Susceptibility of planetary atmospheres to mass-loss and growth by planetesimal impacts: the impact shoreline

M. C. Wyatt¹, ¹★ Q. Kral² and C. A. Sinclair¹

¹*Institute of Astronomy, University of Cambridge, Madingley Road, Cambridge CB3 0HA, UK*

²*LESIA, Observatoire de Paris, Université PSL, CNRS, Sorbonne Université, Univ. Paris Diderot, Sorbonne Paris Cité, 5 place Jules Janssen, F-92195 Meudon, France*

Accepted 2019 October 22. Received 2019 September 18; in original form 2019 April 2

ABSTRACT

This paper considers how planetesimal impacts affect planetary atmospheres. Atmosphere evolution depends on the ratio of gain from volatiles to loss from atmosphere stripping f_v ; for constant bombardment, atmospheres with $f_v < 1$ are destroyed in finite time, but grow linearly with time for $f_v > 1$. An impact outcome prescription is used to characterize how f_v depends on planetesimal impact velocities, size distribution, and composition. Planets that are low mass and/or close to the star have atmospheres that deplete in impacts, while high-mass and/or distant planets grow secondary atmospheres. Dividing these outcomes is an $f_v = 1$ impact shoreline analogous to Zahnle and Catling’s cosmic shoreline. The impact shoreline’s location depends on assumed impacting planetesimal properties, so conclusions for the atmospheric evolution of a planet like the Earth with $f_v \approx 1$ are only as strong as those assumptions. Application to the exoplanet population shows that the gap in the planet radius distribution at $\sim 1.5 R_\oplus$ is coincident with the impact shoreline, which has a similar dependence on orbital period and stellar mass to the observed gap. Given sufficient bombardment, planets below the gap would be expected to lose their atmospheres, while those above could have atmospheres enhanced in volatiles. The level of atmosphere alteration depends on the total bombardment a planet experiences, and so on the system’s (usually unknown) other planets and planetesimals, though massive distant planets would have low accretion efficiency. Habitable zone planets around lower luminosity stars are more susceptible to atmosphere stripping, disfavoured M stars as hosts of life-bearing planets if Earth-like bombardment is conducive to the development of life.

Key words: planets and satellites: atmospheres – circumstellar matter – planetary systems.

1 INTRODUCTION

There are now over 4000 known exoplanets. Many are seen to transit in front of their host stars, enabling study of their atmospheres. Atmosphere characterization is possible not only for gas giant planets (Charbonneau et al. 2002), but also for Earth-sized planets in the habitable zone (e.g. de Wit et al. 2018). Characterization of exoplanet atmospheres is expected to become easier as planets are found to transit around brighter stars (e.g. Rauer et al. 2014; Huang et al. 2018), and it is within our reach to search for evidence of extraterrestrial life in exoplanet atmosphere observations (e.g. Kaltenegger 2017; Defrère et al. 2018). As such, it is important to understand the processes responsible for the origin and evolution of planetary atmospheres (Kasting & Catling 2003). Not only will this help with the interpretation of exoplanet atmosphere observations,

in turn constraining those formation and evolution processes, but it will also allow consideration of issues such as how conditions on planetary surfaces evolve. It is not yet fully understood how these processes played out on the Solar system’s terrestrial planets (e.g. Prinn & Fegley 1987; Lammer et al. 2018), which nevertheless provide valuable constraints, particularly in the regime of low-mass and/or habitable planets.

In general, it might be considered that a planet could acquire an atmosphere during its formation, by accretion of either gas from the protoplanetary disc (predominantly H or He; Lammer et al. 2014), or solids containing volatiles (such as water or CO₂) that are outgassed during accretion (Elkins-Tanton & Seager 2008). That atmosphere could then evolve due to internal processes, such as the dissipation of the planet’s initial gravitational and thermal energy (which promote atmospheric mass-loss), outgassing of volatiles originally locked within the planet (Craddock & Greeley 2009; Elkins-Tanton 2012; Godolt et al. 2019), and geological processes such as the subduction

* E-mail: wyatt@ast.cam.ac.uk

of CO₂ (e.g. Walker, Hays & Kasting 1981; Zahnle et al. 2007). External processes could also be at play, such as irradiation by the central star (which also promotes atmospheric mass-loss through photoevaporation) and impacts from planetesimals (which can both strip the atmosphere and deliver volatiles to it).

The broad properties of the exoplanet population can be explained with a subset of the processes mentioned above. For example, the core accretion paradigm in which giant planets accrete significant atmospheres once their cores reach $\gg 1-10 M_{\oplus}$ (Pollack et al. 1996; Brouwers, Vazan & Ormel 2018) is successful at explaining the distribution of planetary masses and radii (e.g. Jin & Mordasini 2018). Planets smaller than $1.6 R_{\oplus}$ are inferred to have (at most) tenuous atmospheres, while those up to $\sim 4 R_{\oplus}$ have atmospheres with a few per cent by mass, though there is some degeneracy when inferring atmosphere mass depending on whether the planet's mass is dominated by volatiles (Rogers 2015; Lozovsky et al. 2018). There is direct evidence for photoevaporative mass-loss in some systems (e.g. Vidal-Madjar et al. 2003), which when applied to the broader population can explain the absence of large planets at small orbital distances (e.g. Lecavelier Des Etangs 2007). Most recently, a gap in the distribution of planetary radii at $\sim 1.5 R_{\oplus}$ (Fulton et al. 2017; Van Eylen et al. 2018) has also been explained by photoevaporation by stellar X-rays that are prevalent during the first 100 Myr or so of a star's life (Jackson, Davis & Wheatley 2012); more massive atmospheres are not lost on this time-scale and so can be retained, while those below this level are destroyed (Lehmer & Catling 2017; Owen & Wu 2017). An alternative explanation for this gap has also been given as mass-loss driven by the luminosity of the cooling core (Ginzburg, Schlichting & Sari 2018).

A similar story applies to the planets and moons in the Solar system, for which the presence or absence of an atmosphere is determined by the ratio of insolation to escape velocity to the fourth power, creating a *cosmic shoreline* that may be explained by hydrodynamic thermal escape or irradiation (Zahnle & Catling 2017). However, Solar system studies also highlight the potential contribution of impacting planetesimals (e.g. Cameron 1983; Ahrens 1993). For example, Zahnle et al. (1992) noted that the difference between Titan's atmosphere and the lack of one on Ganymede and Callisto could be explained by the lower impact velocity on to Titan, which can thus retain an impact-generated atmosphere, and impacts are thought to be responsible for the erosion of Mars' primordial atmosphere (Melosh & Vickery 1989). Indeed, Zahnle & Catling (2017) note that the cosmic shoreline may alternatively be explained by impact erosion, but do not consider that possibility in as much detail because of uncertainties in how to model this. The Earth's atmosphere is also thought to have been affected by impacts, having its origin in a combination of gas from the protosolar nebula and accreted cometary volatiles (Owen & Bar-Nun 1995; Dauphas 2003), with impacts also postulated as the origin of the Earth's oceans (Chyba 1990), as well as a means of delivering organic molecules (Chyba et al. 1990). This interpretation is, however, challenged by the detailed volatile compositions of the Earth and comets, which suggest that comets are not the dominant reservoir (Marty et al. 2016), though the picture for noble gases is more complicated (Marty et al. 2017; Zahnle, Gacesa & Catling 2019).

Clearly, there are many competing processes that affect atmosphere evolution. This paper focuses on one of those processes, which is the effect of planetesimal impacts, both their role in stripping a pre-existing atmosphere, and in delivering volatiles to replenish that atmosphere. These processes have previously been applied to consideration of the evolution of Solar system

terrestrial planets (e.g. Melosh & Vickery 1989; Svetsov 2007; de Niem et al. 2012; Schlichting, Sari & Yalinewich 2015; Pham & Karatekin 2016). However, there are differences in the prescriptions for the outcome of collisions between these studies, as well as in their assumptions about the impactors, which lead to slightly different conclusions. These studies are nevertheless converging on the most appropriate prescription, with analytical considerations of the underlying physics of impacts (Schlichting et al. 2015) in broad agreement with numerical simulations (Shuvalov 2009), for example in the conclusion that mass-loss should be dominated by impacts with planetesimals a few km in size. Giant impacts are generally considered to play a less significant role in atmosphere evolution (e.g. Genda & Abe 2003; Schlichting & Mukhopadhyay 2018), though these can provide an element of stochasticity to explain different atmosphere properties seen in the same system (Griffith & Zahnle 1995; Biersteker & Schlichting 2019), and may promote degassing explaining some features of the atmosphere of Venus (Gillmann, Golabek & Tackley 2016).

While the parametrization of Shuvalov (2009) can be extended across a wide range of parameter space, these models for impact-driven atmosphere evolution have not yet been applied to the broader range of planets in the exoplanet population, except in the case of the TRAPPIST-1 planetary system (Kral et al. 2018). This paper aims to address exactly this topic, for example to consider the possibility of an impact shoreline that determines whether planets (and moons) have an atmosphere. It starts in Section 2 by considering how atmospheres evolve with a very basic prescription for the outcome of impacts. The simulations of Shuvalov (2009) are then used in Section 3 to develop a more detailed model that is applied to atmospheres across a broad range of planet masses and distances from stars of different types. The results are summarized in Section 4, where the model is also applied to the exoplanet population to consider what effect impacts may have on their observable properties, and to the Solar system planets to consider how conclusions for atmosphere evolution depend on assumptions about the impacting planetesimals.

2 SIMPLE ATMOSPHERE EVOLUTION MODEL

Consider a model in which a planet's atmosphere has a total mass $m = m_p + m_v$, which is made up of a primordial component (m_p) and a volatile component (m_v) that is delivered later (to replenish a secondary atmosphere) by planetesimal impacts that also lead to atmospheric mass-loss. We will assume that atmospheric mass is lost at a rate \dot{m}^- and that volatiles are delivered at a rate \dot{m}_v^+ , so that $\dot{m} = \dot{m}_v^+ - \dot{m}^-$ and $\dot{m}_p = -(m_p/m)\dot{m}^-$.

If both of these rates are constant, the resulting evolution of the atmospheric mass is

$$m/m_0 = 1 + (f_v - 1)t/t_0, \quad (1)$$

$$m_p/m_0 = (m/m_0)^{1/(1-f_v)}, \quad (2)$$

and $m_v = m - m_p$, where m_0 is the initial atmospheric mass (all of which is primordial), $f_v = \dot{m}_v^+/\dot{m}^-$ is the ratio of atmospheric mass gain and loss rates, and $t_0 = m_0/\dot{m}^-$ is the time it would take to deplete the primordial atmosphere in the absence of any gain from volatile delivery.

The evolution from this simple model is plotted in Fig. 1 for a range of its only free parameter f_v . While this oversimplifies the problem, since these rates (\dot{m}_v^+ and \dot{m}^-) are expected to have a dependence on atmospheric mass that is itself varying, it serves to

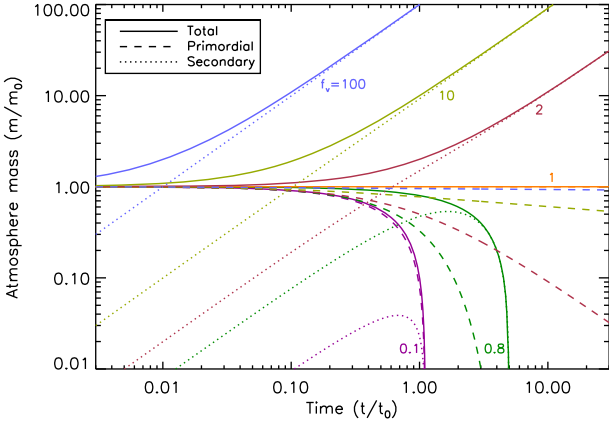


Figure 1. Simple model for the evolution of atmospheric mass in which the rates of gain (due to accretion of volatiles that replenishes a secondary atmosphere) and loss (which depletes both primordial and secondary atmospheres) are assumed to be constant. The evolution depends only on the ratio of the gain and loss rates given by the parameter f_v , six different values of which are shown with different colours as noted in the annotation. The solid lines show the total atmospheric mass, which is made up of a primordial component shown with dashed lines and a secondary component shown with dotted lines.

illustrate an important point. This is that the evolution depends critically on the parameter f_v that determines whether, overall, atmospheres gain or lose mass in planetesimal collisions. If they gain mass (i.e. if $f_v > 1$), then atmospheres grow linearly with time for $t/t_0 \gg 1$ becoming dominated by the secondary component (see e.g. the $f_v = 2, 10$, and 100 lines in Fig. 1). If, on the other hand, they lose mass (i.e. if $f_v < 1$), then while the secondary component starts to grow in mass, this growth will eventually be reversed and the whole atmosphere will deplete to zero in a finite time (see e.g. the $f_v = 0.1$ and 0.8 lines in Fig. 1). Either way, the atmospheric composition becomes more volatile rich with time.

3 PHYSICALLY BASED ATMOSPHERE EVOLUTION MODEL

The model of Section 2 can be improved using a prescription for the outcome of planetesimal impacts. Here, similar to Kral et al. (2018), we use the results of Shuvalov (2009) that considered simulations of planetesimals of sizes in the range 1–30 km impacting at 10–70 km s⁻¹ on to planets that have Earth-like atmospheres. These results can be scaled to arbitrarily large or small impactors, impact velocities and atmospheric densities, in a way that can be understood within a framework that describes the underlying physics (Schlichting et al. 2015). However, care is needed when applying the results outside the range of the original simulations, since the relevant physics may be different for impacts in different regimes. In particular, the Shuvalov (2009) prescription is only valid for impactors that reach a planet’s surface causing a cratering-like event and local atmospheric mass-loss, whereas for small impactors, or for those interacting with very dense atmospheres, the impactors can be decelerated and may fragment or undergo an aerial burst before reaching the surface. At the other extreme, massive impactors can send shock waves through the planet causing non-local atmospheric loss, which is not accounted for by Shuvalov (2009). Aerial bursts have been studied (e.g. Shuvalov et al. 2014), but the prescriptions that are available are not general enough to be useful for this study,

and so such effects are ignored for now, and this caveat will be discussed further in Section 4.3. Giant impacts are discussed in Section 4.2, where it is shown that they only become important for atmospheres that contain a substantial fraction of the planet’s mass.

3.1 Assumptions about planet atmosphere

The starting point of the model is to define the planet’s atmosphere, which is assumed to be isothermal at a temperature $T = 278L_\star^{1/4}a_p^{-1/2}$ K, where L_\star is the stellar luminosity in units of L_\odot and a_p is the semimajor axis in au of the planet’s orbit (which is assumed to be circular). The parameters used in this paper and their units are summarized in Table A1. This temperature sets the scale height of the planet’s atmosphere $H = kT/(\mu m_H g)$, where k is the Boltzmann’s constant, μ is the mean molecular weight of the atmosphere, m_H is the mass of Hydrogen, and $g = GM_p/R_p^2$ is the planet’s surface gravity, M_p is the planet’s mass (which will be in M_\oplus throughout) and R_p its radius (at the solid surface). Note that later equations will be expressed in terms of the planet’s mass and mean density (ρ_p), rather than its mass and radius (these quantities being related by assuming a spherical planet). Later plots will also consider planet density to be $\rho_p = \rho_\oplus = 5.5 \text{ g cm}^{-3}$, though we might equally have included a dependence on mass or composition (e.g. from Lopez & Fortney 2014; Zeng, Sasselov & Jacobsen 2016, a dependence of $\rho_p \propto M_p^{0.19-0.25}$ can be inferred). We will consider two bounding cases for μ , which is that of a primordial (solar) composition $\mu_\odot = 2.35$, and that of a volatile-rich (Earth-like) composition $\mu_\oplus = 29$.

Combining these assumptions gives for the atmospheric scale height

$$H = H_0 L_\star^{1/4} a_p^{-1/2} M_p^{-1/3} \rho_p^{-2/3} \mu^{-1}, \quad (3)$$

where ρ_p is the planet’s density in g cm^{-3} , and $H_0 = 0.73 \times 10^6$ m (meaning that these assumptions give $H_\oplus = 8100$ m for the Earth). We will assume $H \ll R_p$ throughout, which for the given assumptions means that the results are applicable to planets with $M_p \gg 0.017 L_\star^{3/8} \rho_p^{-1/2} \mu^{-3/2} a_p^{-3/4}$; this only excludes extremely low mass planets that are very close to the star, which are not seen yet in the exoplanet population and are not considered here. This means that the total atmospheric mass (m) scales with the atmospheric density at the planet’s surface (ρ_0) according to $m \approx 4\pi H R_p^2 \rho_0$, where for the Earth $m_\oplus = 0.85 \times 10^{-6} M_\oplus$. In some of the analysis, the atmosphere mass will be defined by its ratio to the planet mass, $\delta = m/M_p$, with atmospheres starting out with a mass $m_0 = \delta_0 M_p$, and the Earth having $\delta_\oplus = 0.85 \times 10^{-6}$. The above assumptions also mean that the pressure at the planet’s surface is

$$p/p_\oplus = (\rho_p/\rho_\oplus)^{4/3} (M_p/M_\oplus)^{2/3} (\delta/\delta_\oplus), \quad (4)$$

where p_\oplus is the pressure at the Earth’s surface.

For atmospheres significantly more massive than that of the Earth, the assumption that they are isothermal is no longer valid. The outermost regions will still be isothermal for such atmospheres, but there is a significant portion below this which may be adiabatic down to the surface. While simple prescriptions for the structure of such atmospheres exist (e.g. Owen & Wu 2017), here we prefer to leave consideration of massive atmospheres, such as those with $\delta \approx 1$ percent seen in the transiting exoplanet population (e.g. Wolfgang & Lopez 2015; Fulton et al. 2017), to a future study.

3.2 Outcome of individual impacts

The outcome of a collision with a planetesimal of diameter D and density ρ_{imp} at an impact velocity v_{imp} is determined by the dimensionless parameter [called erosional efficiency by Shuvalov (2009)] $\eta = (D/H)^3 [(v_{\text{imp}}/v_{\text{esc}})^2 - 1][\rho_{\text{imp}}\rho_{\text{ps}}/(\rho_0(\rho_{\text{imp}} + \rho_{\text{ps}}))]$, where $v_{\text{esc}} = \sqrt{2GM_p/R_p}$ is the planet's escape velocity, and ρ_{ps} is the density of the planetesimal, which will be assumed to be equal to ρ_p (i.e. the planet is assumed to have a uniform density throughout). Given the assumptions about the planet's atmosphere in Section 3.1, this means that

$$\eta = \eta_0 L_*^{-1/2} a_p M_p^{4/3} \rho_p^{5/3} m^{-1} \mu^2 D^3 (1 + \rho_p/\rho_{\text{imp}})^{-1} \times [(v_{\text{imp}}/v_{\text{esc}})^2 - 1], \quad (5)$$

where $\eta_0 = 0.5 \times 10^{-18}$ for other parameters in the units of Table A1 (i.e. with m in M_\oplus and D in m). For example, $\eta = 8.5 \times 10^{-9} D^3$ for impacts on to the Earth with $v_{\text{imp}}/v_{\text{esc}} = 2$ and $\rho_p/\rho_{\text{imp}} = 2$ (so that the last two parentheses cancel). According to Shuvalov (2009), the atmospheric mass lost due to this impactor per impactor mass [where $m_{\text{imp}} = (\pi/6)\rho_{\text{imp}}D^3$] is given by

$$m_{\text{atmloss}}(D)/m_{\text{imp}} = [(v_{\text{imp}}/v_{\text{esc}})^2 - 1]\chi_a, \quad (6)$$

where $\log \chi_a = -6.375 + 5.239 \log \eta - 2.121(\log \eta)^2 + 0.397(\log \eta)^3 - 0.037(\log \eta)^4 + 0.0013(\log \eta)^5$ for $\log \eta < 6$. To avoid the unphysical extrapolation to large η in the parametrization of Shuvalov (2009), we extrapolate from a fit to their results in the range $\log \eta = 4-6$ to find a prescription for $\log \eta \geq 6$ of $\log \chi_a = 0.4746 - 0.6438 \log \eta$ that is consistent with Schlichting et al. (2015). The mass gain due to this impactor per impactor mass is given by

$$m_{\text{impacc}}(D)/m_{\text{imp}} = [1 - \chi_{\text{pr}}], \quad (7)$$

where $\chi_{\text{pr}} = 0$ for $\eta < 10$, $\chi_{\text{pr}} = \min[0.07(\rho_p/\rho_{\text{imp}})(v_{\text{imp}}/v_{\text{esc}})(\log \eta - 1), 1]$ for $10 < \eta < 1000$, and $\chi_{\text{pr}} = \min[0.14(\rho_p/\rho_{\text{imp}})(v_{\text{imp}}/v_{\text{esc}}), 1]$ for $\eta > 1000$ [$\eta > 1000$ being the *airless* limit noted in Shuvalov (2009), for which atmosphere drag is negligible for plume expansion].

The prescriptions from equations (6) and (7) are shown in Fig. 2. The large-scale features of this figure were discussed in Shuvalov (2009) and Schlichting et al. (2015). That is, atmospheric mass-loss is most efficient for planetesimals in the middle of the size range (approximately km-sized for Earth-like atmospheres), because larger planetesimals can only remove up to the atmospheric mass in the local vicinity of the impact (i.e. the polar cap), while smaller planetesimals do not impart sufficient energy to the atmosphere to remove significant mass. For example, Fig. 2 shows that the most erosive planetesimals for $v_{\text{imp}}/v_{\text{esc}} = 10$ remove approximately twice their own mass from the atmosphere. Similarly, all of the mass of small planetesimals is retained, but for larger planetesimals much of their mass is lost from the planet as it has too much energy to remain bound (except at very low impact velocities). Setting equation (7) to zero shows that this transition occurs at the size for which $\eta = \eta_{\text{maxret}}$, where

$$\eta_{\text{maxret}} = 10^{1+14(v_{\text{esc}}/v_{\text{imp}})(\rho_{\text{imp}}/\rho_p)} \quad (8)$$

for $v_{\text{imp}}/v_{\text{esc}} > 7.1\rho_{\text{imp}}/\rho_p$ (and $\eta_{\text{maxret}} = \eta_{\text{max}}$ for lower impact velocities).

Fig. 2 highlights that the most important free parameter that determines mass-loss and gain by the planet in this prescription is the ratio of the impact velocity to the planet's escape speed. Larger impact velocities result in both greater levels of atmospheric

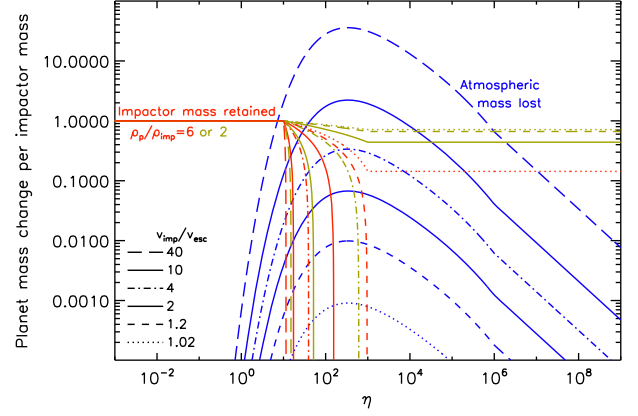


Figure 2. Change in planet mass due to a collision with an impactor at different levels of impact velocity relative to the planet's escape speed shown with different lines. Atmospheric mass lost per impactor mass is shown in blue, and the fraction of the impactor mass that is retained by the planet is shown in red or green for $\rho_p/\rho_{\text{imp}} = 6$ or 2 , respectively. The x -axis scales with the impactor diameter as given in equation (5). All calculations use the prescription in Shuvalov (2009).

mass-loss and less retention of impactor mass (through a decrease in the impactor size that can be retained). The only other variable is the ratio of the planet's density to that of the impactor, ρ_p/ρ_{imp} , which affects the impactor mass that can be retained. Impactors that have larger densities (e.g. $\rho_p/\rho_{\text{imp}} = 2$ might correspond to asteroid-like objects impacting the Earth) can be retained up to larger sizes than those of lower densities (e.g. $\rho_p/\rho_{\text{imp}} = 6$ might correspond to comet-like objects impacting the Earth).

3.3 Outcome of multiple impacts

To determine the effect of multiple impacts on to a planetary atmosphere requires an assumption about the size distribution of impactors. Here we assume that there is a power-law size distribution of impactors characterized by the exponent α , such that the number in the size D to $D + dD$ is $n(D)dD$, where $n(D) \propto D^{-\alpha}$. An infinite collisional cascade of planetesimals with dispersal threshold independent of size would be expected to have $\alpha = 3.5$ (Dohnanyi 1969), but deviations from this can be expected due to size-dependent strength among others things (see e.g. Wyatt, Clarke & Booth 2011), so we leave this as a free parameter. The distribution is assumed to extend from small objects of size D_{min} up to a size of D_{max} . For now, we will work on the assumption that this range is large enough to have no effect on the mass budget, because mass-loss and gain are dominated by intermediate-sized planetesimals. However, this is discussed further below, since for extreme slopes in the size distribution, or for atmospheres that are (or become) significantly different to that of the Earth, it can be objects at the edges of the size distribution that dominate the atmosphere's mass evolution.

While de Niem et al. (2012) found that the stochastic effect of impacts with large bodies can dominate atmospheric evolution, we assume here that this stochasticity can be ignored, and consider that the mean change in a planet's mass can be obtained by integrating equations (6) and (7) over the aforementioned size distribution (as in Kral et al. 2018). The possibility of stochasticity, and the effect of giant impacts more generally, is considered in Section 4.2.

If the total mass of impactors that collide with a planet is m_{ac} , the atmospheric mass-loss and impactor mass retained per m_{ac} are

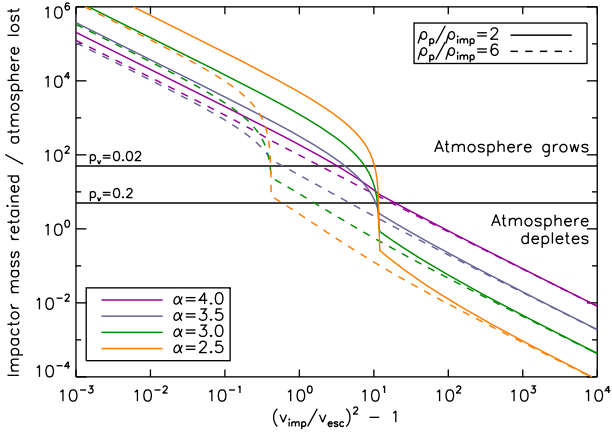


Figure 3. Ratio of total impactor mass retained to atmospheric mass lost for impacts from a size distribution as a function of the ratio of impact velocity to escape velocity $v_{\text{imp}}/v_{\text{esc}}$. The solid and dashed lines are for planet-to-impactor density ratios of $\rho_p/\rho_{\text{imp}} = 2$ and 6, respectively. The different colours are for different slopes in the size distribution α , which is assumed to extend from $\eta_{\text{min}} = 10^{-3}$ to $\eta_{\text{max}} = 10^9$. All calculations use the prescription in Shuvalov (2009). The growth or depletion of an atmosphere in impacts is determined by whether the plotted ratio is more or less than $1/p_v$, where p_v is the fraction of retained impactor that goes into the atmosphere, two representative values for which are shown with horizontal lines.

$$\frac{m_{\text{atmloss}}}{m_{\text{ac}}} = A \left[\left(\frac{v_{\text{imp}}}{v_{\text{esc}}} \right)^2 - 1 \right] \int_{\eta_{\text{min}}}^{\eta_{\text{max}}} \eta^{(1-\alpha)/3} \chi_a d\eta, \quad (9)$$

$$\frac{m_{\text{impacc}}}{m_{\text{ac}}} = A \int_{\eta_{\text{min}}}^{\eta_{\text{max}}} \eta^{(1-\alpha)/3} [1 - \chi_{\text{pr}}] d\eta, \quad (10)$$

$$A = \left(\frac{4 - \alpha}{D_{\text{max}}^{4-\alpha} - D_{\text{min}}^{4-\alpha}} \right) \frac{1}{3} \left(\frac{\eta}{D^3} \right)^{(\alpha-4)/3}, \quad (11)$$

where η_{min} and η_{max} map on to D_{min} and D_{max} , respectively, through equation (5) that is also used to get the ratio η/D^3 in equation (11); for the specific case of $\alpha = 4$, equation (11) needs to be revised to $A = [3 \ln(D_{\text{max}}/D_{\text{min}})]^{-1}$.

Equations (9) and (10) can be used to determine the ratio of impactor mass retained to that lost from the atmosphere, which is shown in Fig. 3 for $\eta_{\text{min}} = 10^{-3}$ and $\eta_{\text{max}} = 10^9$. As long as the range of impactor sizes is large enough for the integrals in these equations to be independent of the boundaries, the resulting ratio depends only on the ratio of the impact velocity to the planet's escape speed ($v_{\text{imp}}/v_{\text{esc}}$), the slope in the size distribution (α), and the ratio of planet to impactor densities (ρ_p/ρ_{imp}). This shows that whether a planet gains or loses mass (i.e. whether the plotted ratio is more or less than unity) is determined primarily by the impact velocity in that mass gain requires small $v_{\text{imp}}/v_{\text{esc}}$. For size distributions in which the mass is dominated by large impactors (i.e. $\alpha < 4$), the ratio shows a sharp increase for low impact velocities $v_{\text{imp}}/v_{\text{esc}} < 7.1 \rho_{\text{imp}}/\rho_p$, since this is the threshold below which all large impactors with $\eta > 1000$ can contribute to mass gain (see equation 7). The magnitude of the increase is greater for distributions that are more strongly weighted towards large impactors (i.e. lower α), and in this regime the ratio inevitably depends on the assumptions about η_{max} . Similar reasons explain why the ratio has a steeper dependence on impact velocity just above this threshold for size distributions with smaller α , in this case because of the increased retention of intermediate-sized impactors. Mass gain is also favoured for higher impactor densities (i.e. smaller ρ_p/ρ_{imp}). The size distribution also plays a

role, in that distributions with impactor mass weighted more towards small planetesimals (i.e. higher α) tend to favour mass gain, since all small planetesimals are retained. However, this trend is reversed (i.e. mass gain is favoured for smaller α) for cases where both impactor velocities are small ($v_{\text{imp}}/v_{\text{esc}} \ll 1$) and impactor densities are high (i.e. small ρ_p/ρ_{imp}), since in this case impactors larger than those that dominate atmospheric mass-loss can be retained; this occurs when $\eta_{\text{maxret}} \gg 10^3$ (see equation 8 and Fig. 2), which given that $v_{\text{imp}}/v_{\text{esc}} \geq 1$ can only happen for small ρ_p/ρ_{imp} . One further consideration is required to determine the effect on the planet's atmosphere, i.e. whether this grows or depletes with time, which is the fraction of the impactor mass that is retained that goes into the atmosphere p_v (see the horizontal lines in Fig. 3).

To quantify the effect of the limits of the integration, we determined from equation (9) the range of η above and below which contributed 10 percent of the total mass-loss (and likewise for impactor retention from equation 10). This showed that, as might be expected from Fig. 2, 80 percent of the atmospheric mass-loss originates in a narrow range of η that depends only on α , which is from $10^{1.8}$ to $10^{4.2}$ for $\alpha = 4$, $10^{2.0}$ to $10^{4.8}$ for $\alpha = 3.5$, and $10^{2.8}$ to $10^{7.8}$ for $\alpha = 2.5$. The impactor mass that is retained comes from a larger range of η that depends on all variables. In particular, for $\alpha \geq 4$ the lower limit of η_{min} cannot be ignored, because all of the mass of impactors smaller than $\eta < 10$ is retained, and for such size distributions the mass is weighted towards the smallest impactors (or is equal in logarithmically spaced bins for $\alpha = 4$). As such, Fig. 3 is only valid for $\alpha = 4$ for the specific case of $\eta_{\text{min}} = 10^{-3}$ and care is needed when considering such steep distributions for which impactor retention likely dominates. For $\alpha = 3.5$, the range of η contributing to impactor mass retention is better defined, and if η_{min} is decreased to arbitrarily low values, it is found that 80 percent of the mass retention comes from a range in η of 10^{-4} up to around 10, but could be higher up to η_{maxret} from equation (8). Since mass retention is weighted to larger η when the impact velocity drops below the threshold of $7.1 \rho_{\text{imp}}/\rho_p$, the η_{max} limit becomes an important consideration for such low velocities, as noted in the previous paragraph. The situation is similar for $\alpha = 2.5$, except that smaller impactors contribute less such that the lower limit is now closer to 10^{-1} . These ranges of η should be used in conjunction with equation (5) to determine whether a given size range falls inside these limits. Thus, the typical range of sizes that contribute to the growth and loss of mass from an Earth-like atmosphere for $\alpha = 3.5$ is 0.02–1 km for growth and 2–20 km for loss.

3.4 Effect of multiple impacts on atmosphere evolution

The results from Section 3.3 can now be used to improve on the model of atmospheric evolution from Section 2. We will return in Section 3.5 to what Section 3.3 predicts for the value of f_v . For now, we note that, for a given scenario, it is reasonable to assume (as was also assumed in Section 2) that f_v remains constant throughout the evolution. This is because f_v can be determined from the ratio plotted in Fig. 3 by multiplying by the fraction of the impactor mass that is retained that goes into the atmosphere (i.e. p_v). The ratio plotted in Fig. 3 has already assumed and then averaged over a given size distribution of impactors (α), and assumed an impactor density (ρ_{imp}), so for a given scenario the plotted ratio just needs to be averaged over the distribution of impact velocities. All of these will depend on the scenario assumed (e.g. the location and mass of the planet, and the provenance of the impactors), but will not depend on the mass of the atmosphere, as long as the size distribution is broad enough, and other parameters like impact velocity appropriate, for

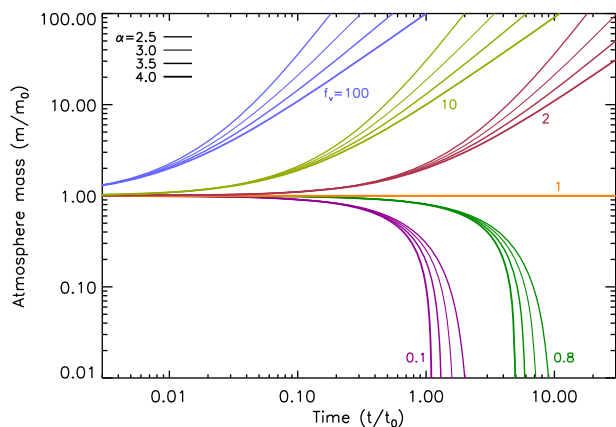


Figure 4. Updated model from Fig. 1 for the evolution of atmospheric mass in which the rates of gain (due to accretion of volatiles that replenishes a secondary atmosphere) and loss (which depletes both primordial and secondary atmospheres) both scale with atmosphere mass. The evolution depends only on the ratio of the gain and loss rates given by the parameter f_v (six different values of which are shown with different colours as noted in the annotation) and the slope in the size distribution α (denoted by the different thickness lines). For clarity, only the total atmospheric mass is shown, since the contribution of the primordial and secondary components can be inferred from Fig. 1, which is identical to that for $\alpha = 4$, and is similar for the other values of α .

the limits in the integrals in equations (9) and (10) to be unimportant. This caveat on the limits of the integrals is important however, since they cannot always be ignored and Section 3.6 considers the situation in which the planet starts with no atmosphere where this is certainly not possible.

What Section 3.3 does show, however, is that the model of Section 2 can no longer assume that mass-loss and gain are independent of time, since equations (9)–(11) show that these should instead be proportional to $m^{(4-\alpha)/3}$. This arises because as the atmosphere decreases in mass it is smaller planetesimals that dominate the atmospheric mass-loss, because the larger planetesimals can only remove the atmosphere in the vicinity of the impact (e.g. Melosh & Vickery 1989); a similar argument applies as the atmosphere grows. We implement this into the model by assuming $\dot{m}^- = \dot{m}_0^-(m/m_0)^{(4-\alpha)/3}$ and $\dot{m}_v^+ = f_v \dot{m}^-$, where \dot{m}_0^- is a constant equal to the initial mass-loss rate. This results in the following evolution:

$$m/m_0 = \left[1 + \left(\frac{\alpha - 1}{3} \right) (f_v - 1)(t/t_0) \right]^{\frac{3}{\alpha-1}}, \quad (12)$$

with m_p from equation (2), $m_v = m - m_p$, and $t_0 = m_0/\dot{m}_0^-$. This evolution is shown in Fig. 4 for $\alpha = [2.5, 3, 3.5, 4]$, and is the same as that of Fig. 1 for $\alpha = 4$ (since this results in mass-loss that is independent of atmospheric mass), noting however that the model is invalid for size distributions with $\alpha \geq 4$ because in this case (as noted in Section 3.3) the lower limit η_{\min} becomes important in the calculation of f_v , which thus varies with time.

Fig. 4 shows that the evolution is not much different with this change. The atmosphere still disappears in a finite time for $f_v < 1$ and grows monotonically with time for $f_v > 1$ and $t/t_0 \gg 1$. The time-scale on which the evolution takes place now depends on the slope in the size distribution, with shallower size distributions (i.e. smaller α , meaning more weighted to large impactors) resulting in atmospheres being lost more slowly or growing more rapidly. However, the sense of faster or slower here is in units of dimensionless

time that is itself dependent on α through the initial mass-loss rate, and so it is not possible from this alone to determine whether the evolution takes more or less real time. Equation (12) shows that the time for the atmosphere to be completely lost for $f_v < 1$ is

$$t_{\text{bare}} = \left(\frac{3}{\alpha - 1} \right) \left(\frac{1}{1 - f_v} \right) \left(\frac{m_0}{\dot{m}_0^-} \right). \quad (13)$$

This means that an $f_v < 1$ planet must accrete a total impactor mass of

$$\Delta m_{\text{ac, bare}} = m_0 \left(\frac{m_{\text{ac}}}{m_{\text{atmloss}}} \right)_0 \left(\frac{3}{\alpha - 1} \right) \left(\frac{1}{1 - f_v} \right) \quad (14)$$

to completely lose its atmosphere, where $(m_{\text{ac}}/m_{\text{atmloss}})_0$ is the inverse of the ratio from equation (9) calculated for the initial atmosphere. This is similar to the mass required to double the atmosphere in the case that $f_v > 1$, which is $[2^{(\alpha-1)/3} - 1]\Delta m_{\text{ac, bare}}$.

To summarize, Fig. 4 can be used to determine the effect of multiple impacts on a planet’s atmosphere. This requires calculation of f_v , which must be done from Fig. 3 as discussed in Section 3.5. Such a calculation is complicated by the fact that the plotted curves need to be averaged over the appropriate distribution of impact velocities and impactor densities, and an assumption needs to be made about the fraction of the impactor mass that is retained that goes into the atmosphere (p_v). There are also a few caveats. First, this assumes that the calculations that go into Fig. 3 are not affected by the largest or smallest impactors in the distribution. Also, this assumes that the evolution in a given time-step can be well described by the average mass-loss, which thus ignores the possible stochastic contribution of single giant impacts (see Section 4.2). Finally, an increase with time of the volatile content of the planet’s atmosphere would increase its mean molecular weight μ . While this would have no effect on f_v , and so whether the atmosphere would ultimately grow or deplete, this would affect the evolutionary time-scale that would get longer as the atmosphere gets more volatile rich. This is because of the reduced atmospheric scale height (equation 3), which results in a decreased mass change per colliding mass (equations 9–11). Some of these complications and caveats will be explored further in Section 3.5 after which the particular case of the evolution of a planet that starts without an atmosphere will be discussed in Section 3.6.

3.5 Determining f_v

As discussed in Section 3.4, calculation of f_v can be done from Fig. 3 by averaging over the appropriate distribution of impact velocities and impactor densities, making also an assumption about the fraction of the impactor mass that is retained that goes into the atmosphere (p_v). The further assumptions about impactor types used in this paper are discussed in Section 3.5.1 before using these in Section 3.5.2 to determine f_v for planets in different regions of parameter space, and considering the sensitivity of the derived f_v to the assumptions in Section 3.5.3.

3.5.1 Assumptions about impactor types

Assumptions in the literature about both impactor densities and the impactor mass retained typically involve an assumption about whether the impacting body is asteroidal or cometary. While this terminology refers to Solar system-like objects, we will apply this more generally here with the following meaning. We will assume asteroidal impactors to have a density of $\rho_{\text{impa}} = 2.8 \text{ g cm}^{-3}$ and that $p_{\text{va}} = 2$ per cent of their mass goes into the atmosphere on impact,

which is based on this being the approximate volatile content of carbonaceous chondrites (e.g. Sephton 2002; Grady & Wright 2003) excluding water that might precipitate on to the surface for planets in the habitable zone (e.g. Zahnle et al. 2007). These volatiles would be in the form of insoluble organic macromolecular material, soluble organics, and carbonates, and may be expected to be degassed during impacts leading to atmospheres rich in H₂O, H₂, CO, or CO₂ (e.g. Schaefer & Fegley 2010). Cometary impactors will be assumed to have a density $\rho_{\text{imp}} = 0.9 \text{ g cm}^{-3}$ with $p_{\text{vc}} = 20$ percent of their mass going into the atmosphere on impact for similar reasons, with the majority of the volatiles in the form of CO, CO₂, and O₂ (excluding water again for the same reason as for asteroidal impactors), and a smaller fraction in molecules such as methane, ethane, methanol, formaldehyde, ammonia, hydrogen cyanide, and hydrogen sulphide (e.g. Mumma & Charnley 2011; Rubin et al. 2019). These assumptions should serve to indicate outcomes for two different types of impactor, but are not supposed to represent the only possible impactor types.

The distribution of impactor velocities is usually taken from N -body simulations of impactor populations as they interact with a planetary system. Since such simulations require an assumption about the source of the impactors and the planetary system that results in them evolving on to orbits that can result in a collision with the planet in question, we prefer to avoid detailed simulations here. Rather we base the expected range of impactor velocities on the following analytical considerations (see also Kral et al. 2018). Consider a planet of mass M_p on a circular orbit at a_p interacting with an impactor on a comet-like orbit, which here we take to mean one with an eccentricity that is close to 1. The impactor's orbital velocity at the location of the planet is approximately $\sqrt{2}v_p$, where $v_p = \sqrt{GM_\star/a_p}$ is the orbital velocity of the planet. If the inclination of the impactor's orbit relative to that of the planet is small, then their relative velocity on approach to impact is $[3 - 2\sqrt{2q/a_p}]^{1/2}v_p$, where q is the impactor's pericentre distance. This relative velocity is thus in the range $(\sqrt{2} - 1)v_p$ (if the comet is close to pericentre at impact) to $\sqrt{3}v_p$ (if the comet's pericentre is far inside the planet's orbit), i.e. $(0.4\text{--}1.7)v_p$. Impactors that originated in an asteroid belt or indeed from the vicinity of the planet in question may have a lower relative velocity at impact, of the order of $\sqrt{1.5}v_p$ for distributions with mean eccentricity e and mean inclination $e/2$ (Wetherill & Stewart 1993).

While impact velocities might be expected to come from a distribution, we take one value as being representative for the resulting f_v , which could be derived for a given distribution of impact velocities by implementing this in equations (9) and (10) and then averaging the resulting ratio. Here we assume that the relative velocities are ξv_p , where $\xi_c = 1.0$ for cometary impactors and $\xi_a = 0.3$ for asteroidal impactors, and then account for the effect of gravitational focussing to get for impact velocities

$$v_{\text{imp}}/v_{\text{esc}} = \sqrt{1 + (\xi v_p/v_{\text{esc}})^2}, \quad (15)$$

$$v_p/v_{\text{esc}} = 3.4 M_\star^{1/2} a_p^{-1/2} M_p^{-1/3} \rho_p^{-1/6}, \quad (16)$$

for the units in Table A1. It is worth reiterating that N -body simulations are needed to get an accurate distribution of ξ if the dynamical origin of the impactors is known. For example, our assumed values are slightly more extreme than those that might be inferred for asteroids and comets impacting the Earth during the Late Heavy Bombardment; e.g. figs 6 and 7 of de Niem et al. (2012) suggest (by eye) average values closer to $\xi_a = 0.5$ and $\xi_c = 0.8$. Similarly, fig. 7 of Kral et al. (2018) shows that the distribution of

impact velocities for planets in a chain can depend on the location in that chain, while our simplistic approach overestimates by a factor of 2 the median impact velocity for the outermost planets in the TRAPPIST-1 system (f, g, and h), and underestimates it for the innermost planets. Such details may contribute to any differences in our results to studies using N -body simulations, but this should not affect general trends, and this can be accounted for where N -body simulations are available.

3.5.2 f_v for different planets

We can now determine for our assumptions about asteroidal or cometary impactors what f_v is for planets with different masses, semimajor axes, and densities, with additional free parameters of the stellar mass and the slope in the size distribution of impactors. The top panels of Fig. 5 show the resulting f_v for planets of density 5.5 g cm^{-3} (i.e. Earth-like) orbiting solar-mass stars for the two different impactor types assuming an impactor distribution with $\alpha = 3.5$ between $D_{\text{min}} = 1 \text{ m}$ and $D_{\text{max}} = 100 \text{ km}$ and an atmosphere mass $\delta = 0.85 \times 10^{-6}$ times that of the planet mass (which means it is Earth-like in terms of its relative mass, but not necessarily in terms of its surface pressure, see equation 4). For reference, the locations of known exoplanets¹ and the Solar system planets are also shown. The slope in the contours of equal f_v arises because this ratio is the same for planets with the same ratio of escape velocity to orbital velocity, which is for planets for which $M_p \propto a_p^{-3/2}$ (see equation 16). This essentially shows the susceptibility of planets in different regions of parameter space to erosion or growth by planetesimal impacts, since as noted in Section 3.4, this determines whether the atmospheres grow or deplete given sufficient impacts. The $f_v = 1$ division between the different outcomes we call the impact shoreline, by analogy with the cosmic shoreline discussed in Zahnle & Catling (2017).

Comparison of asteroidal and cometary impactors (left- and right-hand panels in Fig. 5) shows that planets are more susceptible to mass-loss for impactors with the assumed cometary properties, because the additional volatile content of such impactors is not sufficient to offset the destructiveness of their greater impact velocity. Thus, for the given assumptions, the Earth's atmosphere and that of Venus would be expected to grow in collisions with asteroids, but to deplete in collisions with comets, while all impacts would deplete the atmospheres of Mars and Mercury. For the given assumptions, the atmospheres of many of the known exoplanets would be predicted to grow in all types of planetesimal impacts. This means that, should they have undergone significant bombardment (which will be quantified in the next sections), their atmospheres may be more massive or more volatile rich compared to their primordial values. However, planets that are close enough to the star, in particular those that underwent bombardment by comet-like impactors, would have had their atmospheres stripped.

3.5.3 How f_v changes with different assumptions

While a specific atmosphere mass and upper and lower limits to impactor size were assumed when making the top panels in Fig. 5, for the reasons given in Section 3.3 these should have little effect on the resulting calculation of f_v , in the sense that the outcome would have been very similar with different atmosphere masses

¹Taken on 2018 November 28 from the exoplanet.eu data base (Schneider et al. 2011).

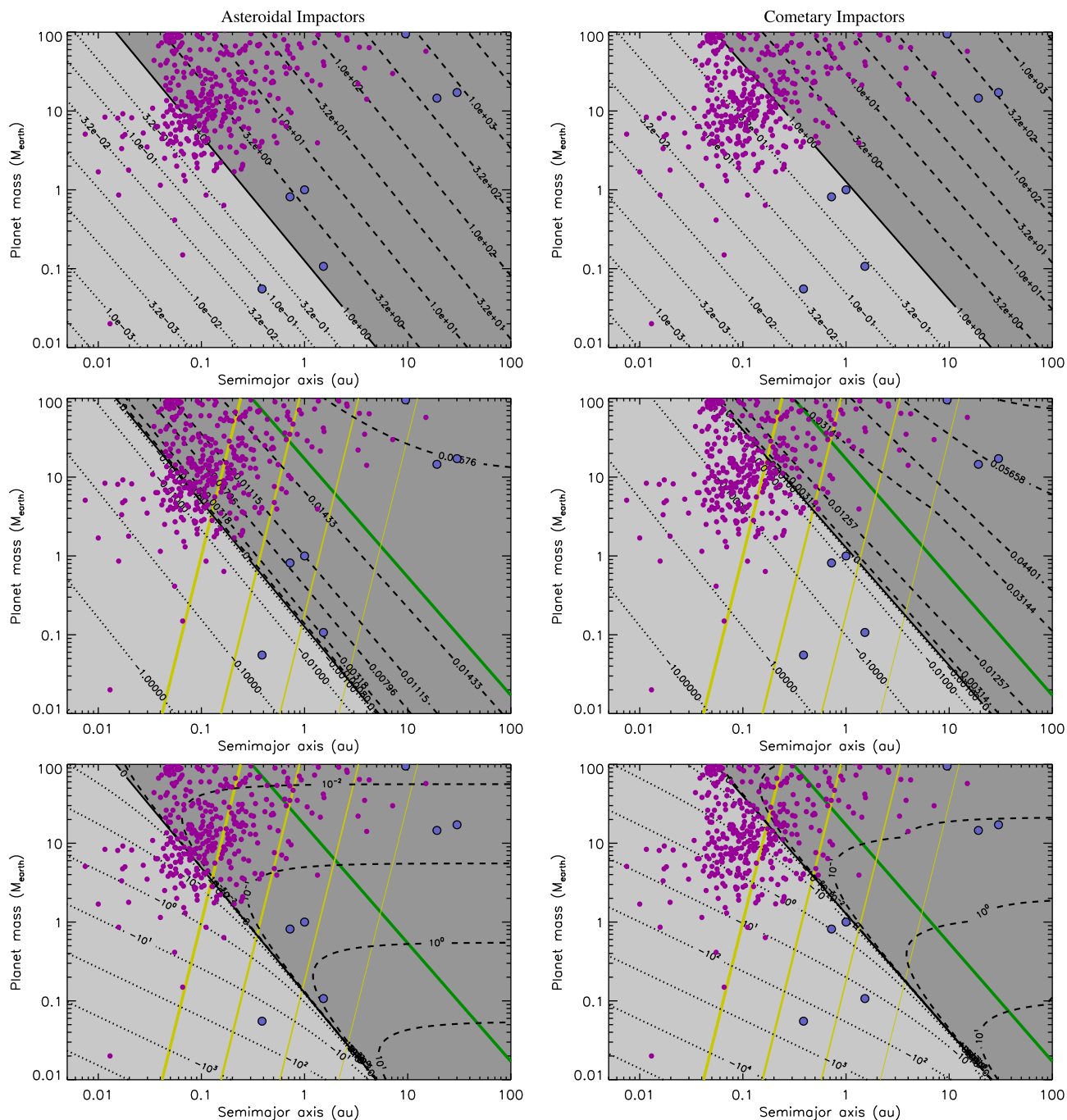


Figure 5. Outcome of impacts with planets of different masses and semimajor axes orbiting $1 M_{\odot}$ stars. The left column assumes asteroidal impactors ($\rho_{\text{imp}} = 2.8 \text{ g cm}^{-3}$ with 2 per cent volatiles and relative velocities approaching impact of 0.3 times the planet’s orbital velocity), while the right column assumes cometary impactors ($\rho_{\text{imp}} = 0.9 \text{ g cm}^{-3}$ with 20 per cent volatiles and relative velocities approaching impact of 1.0 times the planet’s orbital velocity). In all the panels, an impactor size distribution with $\alpha = 3.5$ from $D_{\text{min}} = 1 \text{ m}$ to $D_{\text{max}} = 100 \text{ km}$ is assumed, and the planet is assumed to have a density 5.5 g cm^{-3} , and a $\mu = 29$ atmosphere with a mass 0.85×10^{-6} that of the planet. In the top row, contours show the ratio of atmospheric mass gain (due to volatile retention) to mass-loss (due to atmosphere stripping) in planetesimal impacts, i.e. f_v . In the middle row, contours show the change in atmosphere mass per accreted impactor mass, i.e. $\Delta m / \Delta m_{\text{ac}}$. In the bottom row, contours show the fractional change in atmosphere mass after accreting $m_{\text{ac}} = 3 \times 10^{-5} M_{\oplus}$. The solid black line is the impact shoreline; the atmospheres of planets above this line (i.e. in the darker shaded region where contours are dashed) gain mass in collisions, while those below (i.e. in the lighter shaded region where contours are dotted) lose mass. The dark green line is that for $v_{\text{esc}}/v_p = 1$ above which the planet is more likely to eject planetesimals it interacts with than be impacted by them. The lighter green lines are for constant accretion time-scale from a comet-like population, where that time-scale for the lines from left to right (from thicker to thinner lines) is 0.3 Myr, 30 Myr, 3 Gyr, and 300 Gyr. The accretion efficiency is reduced for planets with longer collision time-scales, since it is more likely that other processes remove planetesimals from the vicinity of the planet before impacts occur. The purple circles are known exoplanets for $0.6\text{--}1.4 M_{\odot}$ stars (from the exoplanet.eu data base on 2018 November 28, Schneider et al. 2011). The larger blue circles are the Solar system planets.

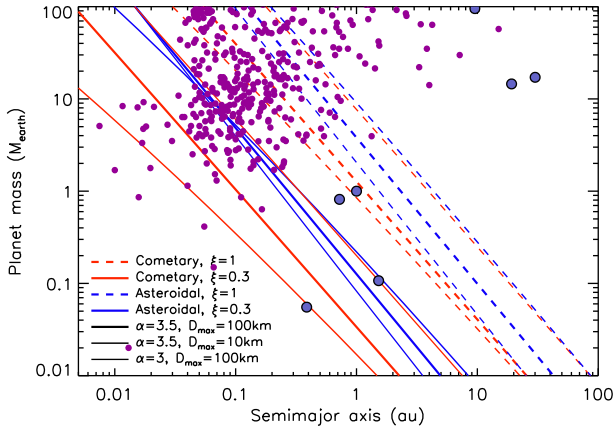


Figure 6. The dependence of the impact shoreline on impactor assumptions. The lines delineate between atmospheres that grow (upper right) and deplete (bottom left) in impacts for planets orbiting Sun-like stars. Different assumptions about the impactors are shown with different lines. Asteroidal impactors ($\rho_{\text{imp}} = 2.8 \text{ g cm}^{-3}$ with 2 per cent volatiles) are shown with blue lines and cometary impactors ($\rho_{\text{imp}} = 0.9 \text{ g cm}^{-3}$ with 20 per cent volatiles) with red lines. The solid lines are for relative velocities near impact 0.3 times the planet’s orbital velocity, while the dashed lines have those relative velocities equal to the planet’s orbital velocity. The lines of different thicknesses indicate different assumptions about the slope in the impactor size distribution (α) and maximum impactor size (D_{max}) as shown in the legend (in all cases, $D_{\text{min}} = 1 \text{ m}$ is assumed). For all the lines, the planet is assumed to have a density 5.5 g cm^{-3} , and a $\mu = 29$ atmosphere with a mass 0.85×10^{-6} that of the planet.

(if not too different, see Section 3.6) and with the assumption that the size distribution had extended to arbitrarily large and small values. A finite upper or lower limit to impactor sizes can become important, however, in certain circumstances. For example, given the dominating impactor sizes noted at the end of Section 3.3 for the Earth (i.e. 0.02–1 km for impactor retention and 2–20 km for atmosphere loss), an upper limit on planetesimal size in the 1–10 km range would have the effect of reducing atmosphere loss without affecting its gain resulting in an increase in f_v . Also, Fig. 3 shows that flatter size distributions (i.e. smaller α , weighted more to larger impactors) would result in more disruptive impacts and so a lower f_v . These expectations are confirmed in Fig. 6, which shows the planet for which $f_v = 1$ (i.e. the transition between atmosphere growth and depletion in impacts, or the impact shoreline) for different assumptions about the size distribution with lines of different thickness. That is, the $f_v = 1$ lines move down when D_{max} is decreased (as impacts become less destructive) and up when α is decreased (as impacts become more destructive).

Fig. 6 also shows how the lines of $f_v = 1$ change with the assumptions about the impact velocities and impactor composition. For example, the lines move up as impact velocities are increased from $\xi = 0.3$ to 1.0, because the impacts become more destructive (see Fig. 3), and impacts tend to favour atmosphere growth (the lines move down) as the fraction of volatiles contained in the impactor (p_v) is increased, though impactor density also plays a role in the plotted values (see Fig. 3). Overall, one point to take away from Fig. 6 is that the outcome of collisions (i.e. whether atmospheres grow or deplete in impacts) is sensitive to what is assumed about the impactors, particularly about their impact velocities, but also about their volatile content, and to a lesser extent their size distribution (although the change in Fig. 6 would have been more significant for $D_{\text{max}} = 1 \text{ km}$). Thus, any definitive claims about atmosphere

evolution require these parameters to be well constrained, which is challenging even in the Solar system.

As noted above, much of the spread in the lines in Fig. 6 can be understood purely from Fig. 3. The one parameter that requires further thought is the upper impactor size D_{max} , the consequence of which can be understood by rearranging equation (5), including also the factor from equation (15), to find that the size corresponding to a given η is

$$D \propto \eta^{1/3} m^{1/3} \mu^{-2/3} \xi^{-2/3} M_p^{-2/9} \rho_p^{-4/9} M_*^{-1/3} L_*^{1/6} \times (1 + \rho_p / \rho_{\text{imp}})^{1/3}. \quad (17)$$

This allows us to determine how the dominating impactor sizes recalled above for the Earth (i.e. 0.02–1 km for impactor retention and 2–20 km for atmosphere loss) change with different assumptions, and so whether this calculation is affected by the impactor size limits. Equation (17) shows that the stellar properties do not play a strong role in how planetesimal size maps on to η (e.g. for the same η for impacts in the TRAPPIST-1 system as for the Solar system, the impactor size is reduced by only 65 per cent), and neither do planet properties (e.g. a factor of 100 increase in planet mass results in a factor of 3 decrease in impactor size for the same η , or less if atmosphere mass scales with planet mass), and neither does the impactor type (e.g. asteroidal impactors are roughly twice the size as cometary impactors for the same η). However, the dependences on m and μ mean that the dominating impactors are 100 times larger than found for the Earth for an atmosphere with $\delta = 1$ per cent of the mass of the Earth and solar composition. This means that more massive atmospheres are more susceptible to growth and that, if the upper size cut-off is in a regime where this becomes important, the lines would move down in Fig. 6 (since an upper cut-off would then cause a lack of destructive impactors). This would also be the case for a more primordial atmosphere, which conversely means that the increasing volatile fraction of a growing atmosphere could make impactors more harmful potentially stalling its growth.

3.6 Evolution of an atmosphere-less planet

One situation in which a planet’s atmosphere evolution cannot be considered in the manner described in Section 3.4 is that in which the planet starts without an atmosphere, i.e. $m_0 = 0$. This is a situation in which the limits of the integrals cannot be ignored, since for the smallest and largest impactors alike $\eta \rightarrow \infty$ (equation 5). To determine what happens in this case, we first consider whether impacts are able to leave any mass in the atmosphere. For low impact velocities, $v_{\text{imp}}/v_{\text{esc}} < 7.1 \rho_{\text{imp}}/\rho_p$, no mass is retained and so no atmosphere growth is possible and the planet will remain forever atmosphere-less.

For impact velocities above this limit, atmosphere growth will be possible, since $f_v \rightarrow \infty$, at least initially. While the atmosphere mass remains small, η_{min} will be large (this could mean, e.g. that $\eta_{\text{min}} \gg 10^6$), which would mean from Fig. 2 that mass gain exceeds mass-loss for all impactor sizes and so f_v must be greater than unity. Thus, the atmosphere would grow with continued bombardment. As the mass of the atmosphere increases, η_{min} (and η_{max}) would decrease, and the atmospheric mass lost per impactor mass also grows (as there is more atmosphere to lose) with little change in the mass gain per impactor. This causes f_v to decrease from its initially high value. Eventually, the atmosphere will have grown such that η_{min} is small and irrelevant, at which point f_v may be greater than or less than unity. There may be turning points in the value of f_v as a

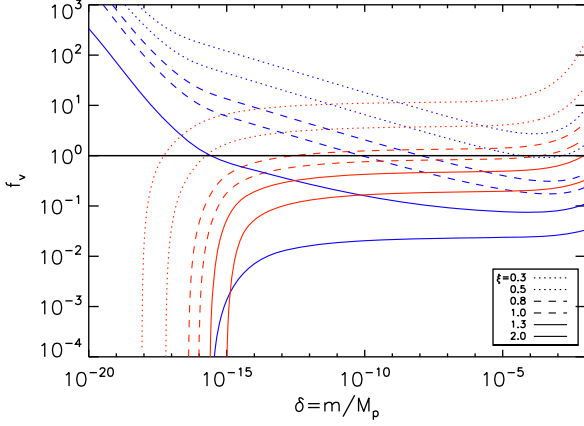


Figure 7. Dependence of f_v on atmosphere mass for an Earth-like planet ($1 M_{\oplus}$, 5.5 g cm^{-3} , 1 au , and $\mu = 29$) orbiting a Sun-like star, being impacted by 1 m – 100 km planetesimals with a size distribution $\alpha = 3.5$. Impactor compositions are assumed to be either asteroidal ($p_v = 0.02$, $\rho_{\text{imp}} = 2.8 \text{ g cm}^{-3}$, blue lines) or cometary ($p_v = 0.2$, $\rho_{\text{imp}} = 0.9 \text{ g cm}^{-3}$, red lines). The legend gives the assumed impact velocity in terms of ξ .

function of atmosphere mass. If f_v remains above unity throughout, then the atmosphere will continue to grow indefinitely. If f_v drops below unity, then atmosphere growth will stall at the value where f_v first reaches unity, since if it grew further then f_v would be less than unity and further impacts would cause atmosphere loss until f_v had increased to unity again (i.e. $f_v = 1$ is a stable equilibrium point if $df_v/d\delta < 0$ at this point).

To illustrate this, Fig. 7 shows how f_v depends on atmosphere mass for the Earth being impacted by planetesimals of asteroidal and cometary composition at different velocities. For bombardment by cometary compositions, the velocities plotted are all above the transition (which occurs at $\xi = 0.24$) and so a bare Earth would always remain as such. For asteroidal compositions, the transition is at $\xi = 1.37$, so for velocities lower than this the atmosphere would grow. For $\xi = 0.5$ – 1.37 , the atmosphere would stall (e.g. at $\delta \approx 10^{-10}$ for $\xi = 1.0$), whereas for $\xi < 0.5$ the atmosphere would continue to grow indefinitely.

It is possible to find a combination of impactor parameters that leads to atmosphere growth that stalls at δ_{\oplus} . However, before reading too much into Fig. 7, a number of uncertainties should be noted. For example, this prediction depends strongly on the assumptions about the outcome of impacts in the airless limit. Comparison with other prescriptions (e.g. Cataldi et al. 2017) and simulations (e.g. Zhu et al. 2019) in this limit shows that the Shuvalov (2009) prescription we are using is reasonable, but may not capture all of the relevant details. Also, the atmosphere masses in question are incredibly small, and so the delivery of a single large impactor can be significant, i.e. the evolution of δ may be stochastic rather than monotonic at the levels of interest. It is also worth noting that similar arguments apply to atmospheres that were predicted in Section 3.5 to deplete in impacts, since if f_v increases as the atmosphere depletes (which is necessarily the case for sufficiently low velocities), then these atmospheres would not be completely removed but instead stall at the value for which f_v first goes above unity. In any case, one thing to take away from Fig. 7 is that while f_v does have some dependence on atmosphere mass, and one that is particularly important to consider for very low atmosphere masses, it is also relatively flat over a large range of δ , and so the broad conclusions of the previous sections are still valid.

3.7 Fractional change in atmosphere per cumulative accreted impactor mass

While Section 3.5 considered the susceptibility of a planet’s atmosphere to erosion or growth, such susceptibility does not mean that the atmosphere will completely disappear or grow significantly, as that requires a consideration of the total mass of impacting planetesimals, their effect on the atmosphere, and how that compares with the initial atmospheric mass m_0 . Clearly, these are not factors that are well known even in the Solar system. We can however give the reader a feeling for how such considerations may apply to planets in different regions of parameter space by plotting the model predictions for the ratio of the change in a planet’s atmosphere mass to the mass of impactors accreted, i.e.

$$\Delta m / \Delta m_{\text{ac}} = (m_{\text{atmloss}} / m_{\text{ac}})(f_v - 1), \quad (18)$$

which is shown in the middle panels of Fig. 5. To make these panels, the assumptions about the initial atmosphere mass (i.e. that this was a fraction $\delta = 0.85 \times 10^{-6}$ the mass of the planet) and about the impactor size cut-offs play a more significant role than in the calculation of f_v , as described below.

To explain the results in the middle panels of Fig. 5, and to scale these to situations with different assumptions, note that the two terms on the right-hand side of equation (18) come from equation (9) and the top panels of Fig. 5, respectively. The second term explains the most prominent feature on the middle panels of Fig. 5, which, as noted already, is that whether an atmosphere grows or shrinks with time is dictated by the f_v factor. That is, the region where planetary atmospheres grow in collisions (dashed lines, darker shading) is separated from that where they deplete (dotted lines, lighter shading) by the solid $f_v = 1$ line (the impact shoreline), the location of which has all of the dependences discussed in Section 3.5.3.

Equations (5), (11), and (15) show that

$$m_{\text{atmloss}} / m_{\text{ac}} \propto [D_{\text{max}}^{4-\alpha} - D_{\text{min}}^{4-\alpha}]^{-1} M_{\star}^{\frac{\alpha-1}{3}} L_{\star}^{\frac{4-\alpha}{6}} M_p^{\frac{-\alpha-2}{9}} a_p^{-1} \times \rho_p^{\frac{4\alpha-19}{9}} \delta^{\frac{4-\alpha}{3}} \mu^{\frac{2\alpha-8}{3}} \xi^{\frac{2\alpha-2}{3}} (1 + \rho_p / \rho_{\text{imp}})^{\frac{4-\alpha}{3}}. \quad (19)$$

Since for atmospheres that deplete in collisions $\Delta m / \Delta m_{\text{ac}} \approx -m_{\text{atmloss}} / m_{\text{ac}}$, this means that the contours in the lighter shaded region would be expected to lie along lines of $M_p \propto a_p^{\frac{-9}{\alpha+2}}$, which for the size distribution assumed in Fig. 5 are only slightly steeper than the $f_v = 1$ line. For planets that are far enough to the left of the $f_v = 1$ line (i.e. small close-in planets), their large impact velocity means that impactors are able to remove more atmosphere mass than the planetesimal mass that is accreted. However, for the known exoplanets, the decrease in atmosphere mass is less than the mass that is accreted.

For atmospheres that grow in collisions, $\Delta m / \Delta m_{\text{ac}} \approx m_{\text{impacc}} / m_{\text{ac}}$, which has a similar scaling to equation (19) but with some slightly different exponents so that this is $\propto M_{\star}^{\frac{\alpha-4}{3}} M_p^{\frac{4-\alpha}{9}} a_p^0 \rho_p^{\frac{4\alpha-16}{9}}$. This explains why the contours of constant $\Delta m / \Delta m_{\text{ac}}$ become flatter in the darker shaded region, and moreover there is little dependence on planet mass. Indeed, the atmosphere mass gain per impactor mass accreted reaches a plateau in the upper right of the middle panels of Fig. 5 at a value that is below p_v (which is the maximum possible since this would require all of the volatiles accreted to go into the atmosphere) by a factor that accounts for the fraction of the impactor mass that arrives in planetesimals that are too large to be retained in the atmosphere.

To rescale the middle panels of Fig. 5 for different assumptions, first note that some of the parameters in the model do not affect

the factor f_v and so their effect on equation (18) is relatively straightforward to determine. For example, as long as the upper size cut-off does not affect the calculation of f_v [i.e. as long as the limits in the size distribution do not contribute to the integrals in equations (9) and (10); see the discussion in Section 3.3] then $\Delta m/\Delta m_{ac}$ scales with δ , μ , and D_{max} in the same way as equation (19), i.e.

$$\Delta m/\Delta m_{ac} \propto \delta^{\frac{4-\alpha}{3}} \mu^{\frac{2\alpha-8}{3}} D_{max}^{\alpha-4}, \quad (20)$$

where the dependence on D_{max} has assumed that $\alpha < 4$. This means that atmospheres that are higher in mass have correspondingly larger changes (or need to accrete more for the same fractional change), as do those that have a more primordial composition (by a factor of 2.3 when changing from the μ_{\oplus} assumed in Fig. 5 to μ_{\odot}). Changing D_{max} can also have a significant effect, because this affects the fraction of the mass that is in the damaging km-sized planetesimal range, noting however that there may be an additional D_{max} dependence not accounted for in equation (20) if this affects the integral in equation (9). While there are significant differences for comparable planets between different impactor types, many of these differences can be understood from the location of the $f_v = 1$ impact shoreline on the top panels of Fig. 5 (see also Fig. 6).

The bottom panels of Fig. 5 show the same information as in the middle panels, but this time recording the fractional change in the planet's atmosphere that would result from accretion of $\Delta m_{ac} = \Delta m_{ac, LHB} = 3 \times 10^{-5} M_{\oplus}$ (i.e. similar to the mass accreted by both the Earth and Mars during the Late Heavy Bombardment; Gomes et al. 2005), i.e. these panels show $(\Delta m/m)/(\Delta m_{ac, LHB}/\Delta m_{ac})$. This is intended to give the reader an idea of whether impacts are likely to have a significant effect on a planet's atmosphere following an epoch of heavy bombardment (although as we will describe below, planets in other systems may experience levels of bombardment that are significantly greater than this, in which case the values in this plot could be scaled accordingly). This shows that for planets with atmospheres that are expected to deplete in impacts (in the lighter shaded region), it is relatively easy to deplete these significantly (i.e. to result in $-\Delta m/m$ of the order of unity or greater). For planets that are expected to grow in impacts (in the darker shaded region), growth can be more modest unless the bombardment was greater than that experienced by the Earth during the Late Heavy Bombardment.

3.8 Cumulative accreted impactor mass per cumulative incoming mass

For a given impactor population (i.e. the incoming planetesimals that have been placed on planet-crossing orbits with a mass m_{inc}), it might be expected that planets in different regions of the parameter space in Fig. 5 would end up accreting different masses (i.e. have a different m_{ac}). Thus, a planet that may appear susceptible to atmosphere growth because of a large positive f_v in the top panels of Fig. 5, and a correspondingly large positive $\Delta m/\Delta m_{ac}$ on the middle panels of Fig. 5, may not grow significantly because it has a low efficiency of accreting the planetesimals that were placed on planet-crossing orbits.

There are two main considerations here. First is that planetesimals encountering planets for which $v_{esc} \gg v_p$ are more likely to be ejected in that encounter than to collide with the planet (e.g. Wyatt et al. 2017). Similarly, the time-scale for planetesimals to collide with planets that are low in mass (or far from the star) can be longer than their dynamical lifetime t_{dyn} , i.e. the time before which other perturbations remove the planetesimals from planet-crossing

orbits (which may be the same perturbations that put them on planet-crossing orbits in the first place, like those from more distant planets or stellar companions). Both effects would result in a low collision efficiency (i.e. a low m_{ac}/m_{inc}), and are hard to quantify because this requires consideration of the other planets in the system that is better suited to study using N -body simulations than analytics (e.g. Kral et al. 2018; Marino et al. 2018).

We could make some progress by deriving a rate at which the planetesimals collide with the planet R_{ac} , the rate at which the planet ejects the planetesimals R_{ej} and assuming some fixed dynamical loss rate R_{dyn} (which is set by the other perturbers in the system). The fraction of the impactor population that is accreted would then be $m_{ac}/m_{inc} = R_{ac}/(R_{ac} + R_{ej} + R_{dyn})$. Indeed, it is possible to derive R_{ac} and R_{ej} for assumptions about the planetesimal orbit (see Kral et al. 2018). However, we refrain from repeating such calculations, since they still require further assumptions about the specific scenario that would obfuscate the generality of what we are trying to achieve here. Instead, we plot a few lines in Fig. 5 that show for which planets efficiency might be expected to be low. One of these is $v_{esc} = v_p$ (the dark green line in Fig. 5), above which ejection starts to dominate over accretion, which is given by

$$M_p = 40 M_{\star}^{3/2} a_p^{-3/2} \rho_p^{-1/2}. \quad (21)$$

The others (the light green lines in Fig. 5) are lines of constant accretion time t_{acc} , calculated assuming that planetesimals interact near the pericentres of their high-eccentricity and low-inclination (~ 0.1 rad) orbits with a planet on a circular orbit, which are given by

$$M_p = 30 M_{\star}^{-3/4} a_p^3 \rho_p Q^{9/4} t_{acc}^{-3/2}, \quad (22)$$

where t_{acc} is in Myr and Q is the planetesimals' apocentre distance in au, which is assumed to be $10a_p$ in the figures. Dynamical removal starts to dominate over accretion below the line for which $t_{acc} = t_{dyn}$ (or equivalently, accretion efficiency drops by a factor of $\sim t_{dyn}/t_{acc}$).

The lines of equations (21) and (22) in Fig. 5 are only meant as a guide, and do not delineate those planets that do and those that do not suffer impacts. For example, while the accretion time for the Earth is ~ 1 Gyr and so 3–4 orders of magnitude longer than the typical dynamical lifetime of comets in the inner Solar system of ~ 0.3 Myr (Levison & Duncan 1997), it was still able to accrete $3 \times 10^{-5} M_{\oplus}$ during the Late Heavy Bombardment (Gomes et al. 2005). This is because the low accretion efficiency $\sim 10^{-6}$ was overcome by a large mass of planetesimals undergoing scattering during this event ($\sim 30 M_{\oplus}$; Gomes et al. 2005). Systems with more regularly spaced planets have higher accretion efficiencies (~ 1 per cent, e.g. Marino et al. 2018), and so can undergo significant accretion without requiring such a major upheaval as the Late Heavy Bombardment. That is, these lines cannot account for the fact that the mass accreted also depends on the ability of external planets to put planetesimals on such orbits among other factors. Nevertheless, these lines show that small planets that are close to the star should have a high collision efficiency, since they might be expected to accrete most planetesimals that are put on planet-crossing orbits, with the caveat that accretion efficiency might still be low if a planet is competing with other nearby planets that also have high accretion efficiencies (as in the TRAPPIST-1 system; Kral et al. 2018).

3.9 Dependence on stellar mass

Fig. 8 shows the same calculations as for Fig. 5, but this time for planets orbiting stars with $M_{\star} = 0.08 M_{\odot}$ and $L_{\star} = 5.2 \times 10^{-4} L_{\odot}$, i.e. with parameters appropriate for the TRAPPIST-1 system (Gillon

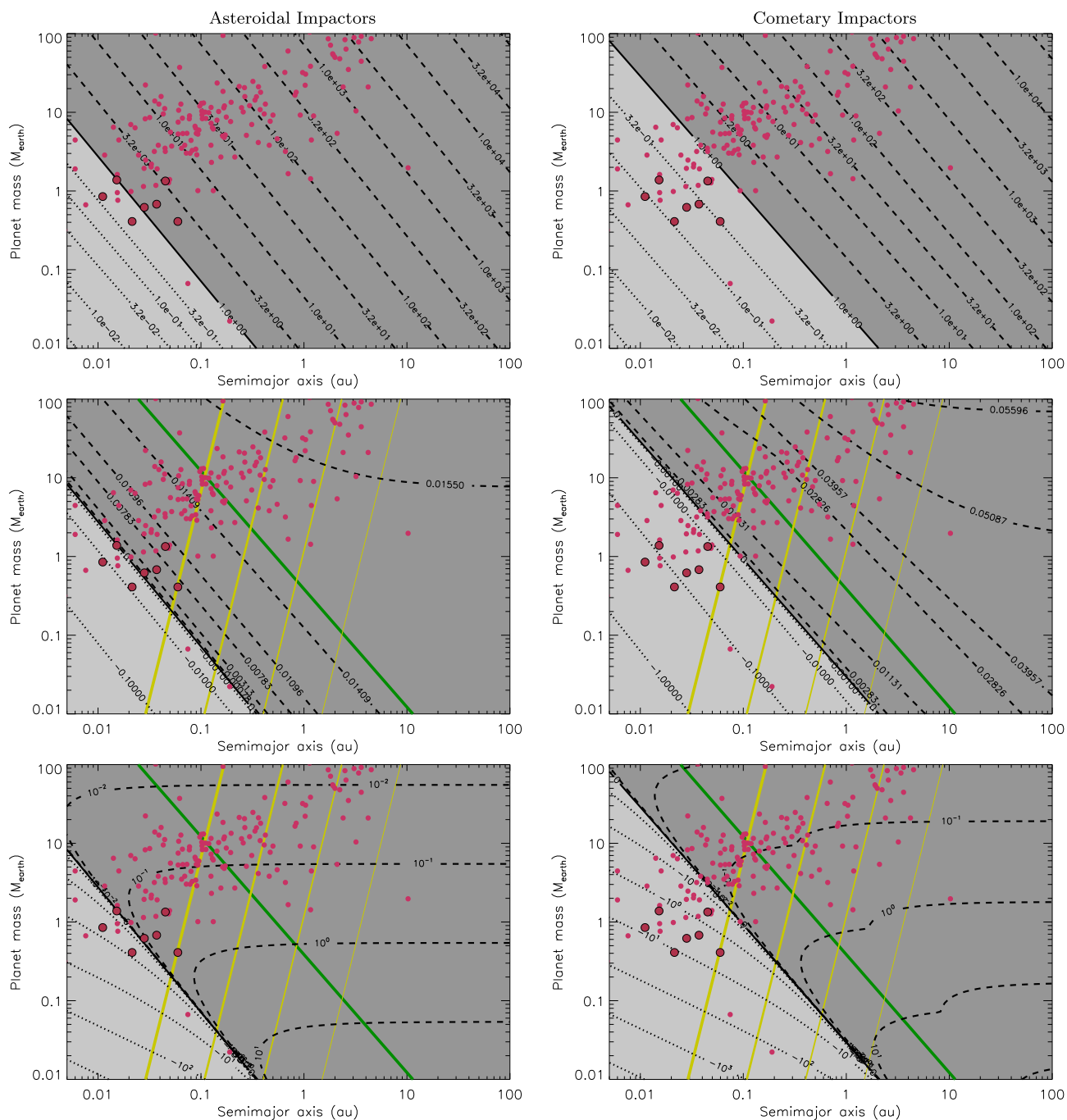


Figure 8. As for Fig. 5 but for planets orbiting $0.08 M_{\odot}$ stars. Here, the red circles are known exoplanets for $<0.6 M_{\odot}$ stars (from the exoplanet.eu data base on 2018 November 28; Schneider et al. 2011), with the seven planets in the TRAPPIST-1 system highlighted by the larger symbols (with parameters from Gillon et al. 2017).

et al. 2017). Comparison of the top panels in the two figures shows how the slower orbital velocity (and so smaller impact velocity) for lower mass stars results in less destructive impacts for planets with the same properties. Nevertheless, the location of the $f_v = 1$ line explains why Kral et al. (2018) concluded that the closest in planets in the TRAPPIST-1 system would have their atmospheres stripped in cometary impacts. Their conclusion that the atmospheres of the outermost planets would grow in collisions is because their calculations made different assumptions about the distribution of

impact velocities (which are more realistic for the scenario they were considering for this system).

4 DISCUSSION

This paper has considered the effect of planetesimal impacts on planetary atmospheres, using assumptions that are valid when the atmosphere is not massive enough for planetesimals to disintegrate before reaching the surface, or for the structure of the atmosphere

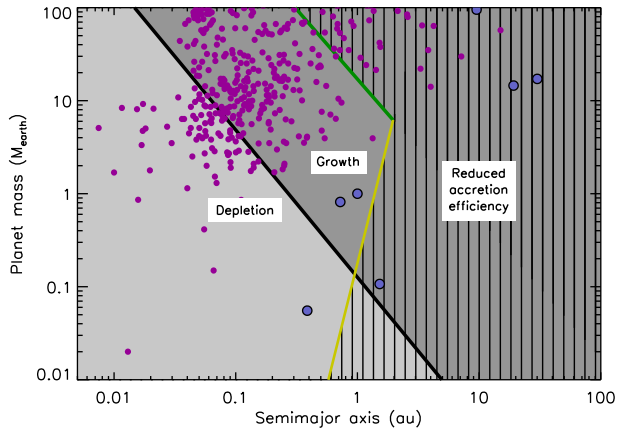


Figure 9. Summary of the different outcomes of bombardment that might be expected for the atmospheres of planets in different regions of parameter space, for planets orbiting solar-mass stars being impacted by asteroidal impactors. The two main regions are that of atmosphere growth (darker shaded region) and depletion (lighter shaded region) that are divided by the impact shoreline shown with the thick black line. However, in the cross-hatched region, a reduced accretion efficiency might lead to less change in atmosphere.

to deviate from our simple prescription, and (justifiably) ignoring the effect of giant impacts. Some starting point for the atmosphere has been assumed, and other factors that may affect the evolution of the atmosphere are ignored, such as photoevaporation due to stellar photons or outgassing of volatiles from the interior that were inherited during formation. While these caveats should be born in mind in the following, these assumptions make it possible to draw some broad conclusions about the effect of planetesimal impacts on planetary atmospheres that are summarized in Section 4.1 before considering how giant impacts or massive atmospheres might affect those conclusions in Sections 4.2 and 4.3, then going on to consider the implications for specific systems in Sections 4.4 and 4.5, as well as the broader implications for the development of life in Section 4.6.

4.1 Summary

The main conclusion of Section 3 is that the planet mass–semimajor axis parameter space can be divided into regions with different outcomes, with some dependence on stellar mass and on the physical and dynamical properties of the impactors. This is illustrated in Fig. 9 that shows lines appropriate for asteroidal impactors on to planets orbiting solar-mass stars, noting that the boundaries between the different regions are not meant to be strictly interpreted.

4.1.1 Planets expected to have no atmosphere (region labelled depletion)

Planets that have $f_v < 1$ and $t_{\text{acc}} \ll 3 \text{ Gyr}$ would be expected to have any primordial atmosphere depleted by bombardment. This applies to planets that are both low in mass and very close to their host stars, a prime example being the innermost planets orbiting TRAPPIST-1 (Kral et al. 2018). The low negative values of $\Delta m/m$ following accretion of $3 \times 10^{-5} M_{\oplus}$ in this regime shown in the bottom panels of Figs 5 and 8 mean that these planets could be expected to completely lose any Earth-like atmospheres when subjected to bombardment levels comparable to that inferred for the Earth during the Late Heavy Bombardment. The bombardment level required for

complete atmosphere loss can be inferred from the middle panels of Figs 5 and 8, since equation (14) shows that

$$\Delta m_{\text{ac,bare}}/m_0 = 3(\alpha - 1)^{-1}(\Delta m/\Delta m_{\text{ac}})^{-1}, \quad (23)$$

i.e. the mass that needs to be accreted is approximately the atmosphere mass divided by the value plotted in those panels (noting that equation (20) shows that the plotted value would also need to be scaled by $[\delta_0/0.85 \times 10^{-6}]^{0.17}$). The only impediment to these planets having completely lost their atmospheres is either an absence of impactors (i.e. below a level given by the initial atmosphere mass divided by the value plotted in the middle panel of Fig. 5), or for the initial atmospheres to be sufficiently massive (although in such extremes, the assumptions in this paper might break down; see Section 4.3).

4.1.2 Planets expected to have atmospheres enhanced in collisions (region labelled growth)

Planets for which $f_v > 1$ and $t_{\text{acc}} \ll 3 \text{ Gyr}$ and $v_{\text{esc}} < v_p$ would be expected to grow secondary atmospheres in collisions. This applies to planets that are close to the star, more massive than those depleted in collisions discussed in Section 4.1.1, but not so massive that their large escape velocity results in a reduced accretion efficiency. There still needs to be a sufficient level of bombardment for the atmospheres to grow significantly, but the bottom panels of Figs 5 and 8 show that slightly higher than Late Heavy Bombardment levels of accretion would be sufficient to grow an Earth-like atmosphere (in the sense that $\delta = \delta_{\oplus}$) for many such planets. The middle panels of Figs 5 and 8 suggest that atmospheres could grow in mass by typically ~ 1 percent of the impactor mass accreted. Thus, the 1 percent accretion efficiency seen in the simulations of Marino et al. (2018) could result in atmospheres 100 times more massive than that on the Earth for bombardment involving just $1 M_{\oplus}$ of planetesimals, which could be a fraction of any planetesimal belt.

4.1.3 Planets likely unaffected by collisions (region labelled reduced accretion efficiency)

The atmospheres of planets that are either far from the star, or very high in mass, may be largely unaffected by collisions. This is not because they would be unaffected by any collisions that occurred. Indeed, atmosphere growth or depletion is always the favoured outcome in the darker and lighter shaded regions of Fig. 9 (with the caveat that this boundary has some uncertainties as noted in Fig. 6). Rather this is because planetesimals could be removed dynamically from the planet’s vicinity faster than they can undergo collisions, resulting in a low accretion efficiency. Planets that are susceptible to having a low accretion efficiency are identified by having $v_{\text{esc}} > v_p$ and/or $t_{\text{acc}} \gg 3 \text{ Gyr}$. However, it is important to emphasize the caveat that such dynamical removal depends on what other planets are present in the system, and it could be that planets in this region still manage to accrete a significant quantity of planetesimals and so have their atmospheres altered in the way indicated by the shading.

4.2 Giant impacts

The parametrization for χ_a in equation (6) is not applicable to giant impacts for which a planet’s atmosphere is not only lost locally at the point where the impact occurs. Rather giant impacts send a shock wave through the body of the planet, which is transmitted

to the atmosphere. This can accelerate parts of the atmosphere to beyond the escape velocity, leading to partial loss of the atmosphere globally. A prescription for the outcome of giant impacts is that the atmospheric mass lost per impactor mass can be approximated for an isothermal atmosphere by (Schlichting et al. 2015)

$$m_{\text{atmloss,GI}}(x)/m_{\text{imp}} = \delta(v_{\text{imp}}/v_{\text{esc}})[0.4 + 1.4x - 0.8x^2], \quad (24)$$

where $x \equiv (v_{\text{imp}}/v_{\text{esc}})(m_{\text{imp}}/M_p)$; for an adiabatic atmosphere, the coefficients are instead 0.4, 1.8, and -1.2 .

This means that the shock wave caused by a giant impact results in an atmospheric mass-loss per unit impactor mass that typically remains constant (i.e. independent of impactor size) up to very large impactors, at a level that is proportional to the atmosphere-to-planet mass ratio δ times the ratio of impact to escape velocities ($v_{\text{imp}}/v_{\text{esc}}$). This should be added to the local atmospheric mass-loss plotted in Fig. 2, which in contrast decreases rapidly with increasing impactor size. This means that there is a size D_{GI} above which giant impacts dominate atmospheric mass-loss, and below which giant impact erosion can effectively be ignored. This transition can be calculated by equating $m_{\text{atmloss,GI}}$ from equation (24) with m_{atmloss} from equation (6). However, to give the reader a feeling for where this transition occurs, note that the prescription from Schlichting et al. (2015) (which is similar but not identical to that of Shuvalov 2009) puts the boundary at approximately

$$D_{\text{GI}} \simeq \left[1.6H R_p^2 (v_{\text{esc}}/v_{\text{imp}}) (\rho_p/\rho_{\text{imp}}) \right]^{1/3}. \quad (25)$$

The combined effect of multiple giant impacts can be computed by integrating $m_{\text{atmloss,GI}}(x)/m_{\text{imp}}$ over the size distribution of the bodies causing giant impacts (under the assumption that these arrive in steady state). Using the assumed power-law size distribution, the atmospheric mass-loss per unit impactor mass is

$$\frac{m_{\text{atmloss,GI}}}{m_{\text{ac}}} = \delta \frac{v_{\text{imp}}}{v_{\text{esc}}} \left\{ 0.4 + 1.4 \left(\frac{4-\alpha}{7-\alpha} \right) \left[\frac{x_{\text{max}}^{(7-\alpha)/3} - x_{\text{min}}^{(7-\alpha)/3}}{x_{\text{max}}^{(4-\alpha)/3} - x_{\text{min}}^{(4-\alpha)/3}} \right] - 0.8 \left(\frac{4-\alpha}{10-\alpha} \right) \left[\frac{x_{\text{max}}^{(10-\alpha)/3} - x_{\text{min}}^{(10-\alpha)/3}}{x_{\text{max}}^{(4-\alpha)/3} - x_{\text{min}}^{(4-\alpha)/3}} \right] \right\}, \quad (26)$$

which works for all power-law indices except $\alpha = 4, 7$, and 10.

To quantify the regime where it is no longer possible to ignore giant impact-induced atmospheric mass-loss, Fig. 10 shows the atmosphere-to-planet mass ratio δ_{GI} at which giant impact mass-loss (equation 26) is equal to that caused by local effects (equation 9). Unlike Fig. 2 for which the A factors from equations (9) and (10) cancelled, Fig. 10 has had to make assumptions about the star, planet, and impactors, which are noted in the caption. Nevertheless, these plots show that atmospheres have to be a substantial fraction of the planet's mass before giant impact-induced atmospheric mass-loss becomes important, with high-mass planets at large distances from the star being most susceptible to such effects, primarily because of the small relative velocity of impacts in this region. Note that planets in this regime were expected to grow by impacts when giant impacts were ignored (see the top panels of Figs 5 and 8), so while including giant impacts into the analysis would have the effect of reducing f_v , this would not necessarily reverse the conclusion that impacts would result in the atmospheric growth for such planets. Asteroidal (rather than cometary) impactors also have a greater propensity for atmospheric loss by giant impacts, as do planets around lower mass stars. A planet like the Earth would require its atmosphere to be of the order of 1 percent of the planet mass before giant impacts become important. This explains why Schlichting et al. (2015) concluded that giant impacts

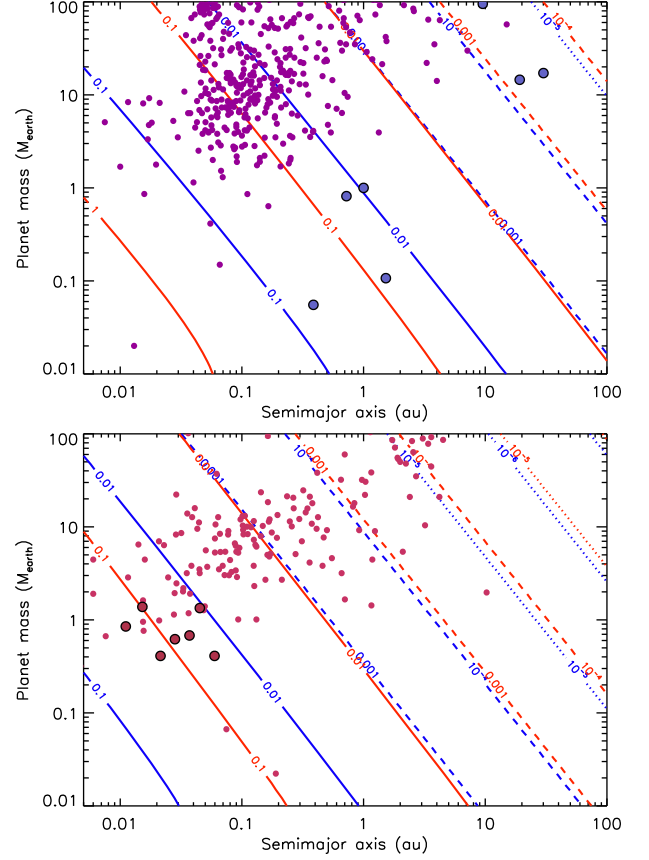


Figure 10. Atmosphere-to-planet mass ratio δ_{GI} above which giant impacts dominate an atmosphere's mass-loss over the local effects of smaller impacts [i.e. the line shows where $m_{\text{atmloss,GI}}(\delta_{\text{GI}}) = m_{\text{atmloss}}(\delta_{\text{GI}})$]. Both the panels assume an impactor size distribution with $\alpha = 3.5$ that extends from $D_{\text{min}} = 1$ m to $D_{\text{max}} = 1000$ km, a planet density of $\rho_p = 5.5 \text{ g cm}^{-3}$, and an atmosphere with a mean molecular weight $\mu = 29$. Asteroidal impactors are shown in blue ($\rho_{\text{imp}} = 2.8 \text{ g cm}^{-3}$ and $\xi = 0.3$), and cometary impactors in red ($\rho_{\text{imp}} = 0.9 \text{ g cm}^{-3}$ and $\xi = 1$). The top panel assumes a star with $M_* = 1 M_\odot$ and $L_* = 1 L_\odot$, while the bottom panel uses $M_* = 0.08 M_\odot$ and $L_* = 5.2 \times 10^{-4} L_\odot$. The line style is simply a function of δ_{GI} , with the solid and dashed lines indicating that giant impacts only dominate in atmospheres that are sufficiently massive for the assumptions in the model to break down.

do not dominate atmosphere erosion, which holds as long as the atmosphere is not too massive.

Individual impacts can have a devastating effect on an atmosphere. This becomes the case when the mass lost in an individual impact is of the order of the atmosphere mass, which occurs when $x \approx 1$ for the prescription of equation (24) (above which the prescription is no longer valid). Thus, individual impactors can only be ignored when the largest impactor has a mass m_{imp} that is much less than $M_p v_{\text{esc}}/v_{\text{imp}}$. That is, the stochastic effect of individual impactors cannot be ignored when impactor masses are close to the mass of the planet (or indeed much smaller if the impact velocity is large enough), and this is independent of how massive the atmosphere is. While such events may be expected to be inevitably rare for most size distributions, their stochastic nature could result in an atmospheric mass different from that predicted in Figs 5 and 8, and in particular this could explain differences in the atmospheres of neighbouring planets that should have undergone similar bombardment histories, or at least ones that

should be different in a predictable way so that any differences in their atmospheres that result from impacts should be relatively well known (e.g. Griffith & Zahnle 1995; Biersteker & Schlichting 2019).

To summarize, the effect of giant impacts can be implemented into models of atmospheric evolution using equation (26) (though it may also be important to consider the contribution to the atmosphere from material vaporized from the planet surface, e.g. Melosh 1989; O’Keefe & Ahrens 1989; Vickery & Melosh 1990; Pope et al. 1997), with the further assumption that impactor retention is unaffected by the additional physics of giant impacts (i.e. this is still given by equation 7). The stochastic effect of individual impacts could also be readily included using Monte Carlo methods (e.g. Griffith & Zahnle 1995; de Niem et al. 2012; Wyatt et al. 2014). However, we conclude that this is unlikely to have a significant effect, except in the case that the atmosphere is already massive (as quantified in Fig. 10), or if the largest impactors are comparable in mass to the planet. It is, however, worth noting that other authors have inferred giant impacts to play an important role in atmosphere evolution (e.g. de Niem et al. 2012). The explanation for this discrepancy seems to be that those studies extrapolated parametrized outcomes derived for <10 km bodies (Svetsov 2007) up to >100 km bodies for which the relevant physics is different, thus requiring different parametrization (see Schlichting et al. 2015). Nevertheless, this highlights that there remain some differences in the literature on the correct approach to modelling the outcomes, which can result in qualitatively different evolution.

4.3 Massive atmospheres

The prescription for the outcome of impacts used in this paper is valid for impactors that reach the planet’s surface. This is inevitably not the case for the smallest impactors, which instead cause aerial bursts or fragment before reaching the surface, changing their effect on the atmosphere. This is particularly relevant for massive atmospheres, like that of Venus, for which this can be relevant for the tens of km-size range of planetesimals that had been predicted to have most effect on the planet’s atmosphere. Simulations in this regime were performed in Shuvalov et al. (2014), which also provided a prescription to implement this in a manner similar to that presented in Section 3.2 (see their equations 7–11). However, since these simulations were only performed for an Earth-like planet, their equations 9 and 10 were not generalized to the range of planet masses being considered here. Nevertheless, their results can be used to give a qualitative understanding of how this would change the results.

The main consequence of aerial bursts is to change Fig. 2 in the regime of impactors smaller than a certain size, which means for $\eta < \eta_{ab}$, where

$$\eta_{ab} = 0.19(\rho_0/\rho_{imp})^{1/2}(1 + \rho_{imp}/\rho_p)^{-1}[(v_{imp}/v_{esc})^2 - 1]. \quad (27)$$

There is also a narrow range of η for which fragmentation before impact is important, extending from η_{ab} up to $\eta_{fr} \approx 4.0\eta_{ab}$. Since η_{ab} has a dependence on the density of the atmosphere, a more massive atmosphere results in larger planetesimals being affected. In the regime where aerial bursts are important, this results in an increased atmospheric loss, i.e. a greater $m_{atmloss}(D)/m_{imp}$, the level of which scales $\propto \eta^{1/3}m^{1/3}$ (among other dependences). That is, the level of mass-loss for a given η depends on the atmosphere mass, which was not the case before, adding an additional parameter to be considered in the analysis. Impactor retention in this regime can be assumed to be 100 per cent.

It is not the purpose of this paper to explore this in detail, but it is worth noting that this prescription could mean that atmosphere growth might stall, as atmosphere loss becomes more efficient as the mass grows.

4.4 Application to the Solar system

Our model was already applied in Section 3.5 to the question of whether the atmospheres of the terrestrial planets in the Solar system grow or deplete in planetesimal collisions. Here we expand on Fig. 5 to consider the effect of a Late Heavy Bombardment-like bombardment level on the current atmospheres of the terrestrial planets (i.e. using the actual planet properties rather than reference values) for the given assumptions about asteroidal or cometary impactors (see Table 1). Thus, the Earth and Venus atmospheres grow by +39 and +0.2 per cent for asteroidal impactors, respectively, but both deplete in cometary impacts, with Mercury also being depleted in all impacts, and Mars depleted in cometary impacts but growing its atmosphere for asteroidal impactors. Further work would be needed to consider the implications of this model for Uranus and Neptune, since while Fig. 5 might suggest that neither planet should have their atmospheres significantly enhanced with an LHB-like level of accretion, that level refers only to that accreted on to the Earth and both planets have $v_{esc} \gg v_p$ and long accretion times suggesting a low accretion efficiency, and moreover the ice giants have atmospheres that are sufficiently massive for the prescription to be invalid.

However, the discussion in Section 3.5.3 already gives reason for caution when interpreting such values, since they are highly sensitive to the assumptions. Here we expand on this point in Fig. 11, which shows how the change in atmosphere mass per impactor mass accreted (i.e. $\Delta m/\Delta m_{ac}$) depends on assumptions about the impactor relative velocity (ξ) and size distribution (α and D_{max}) for asteroidal and cometary impactors (now defined only by their density and contribution to the atmosphere, ρ_{imp} and p_v). This shows how changing the impactor relative velocity from $\xi = 0.3$ to 0.5 for asteroidal impactors and from $\xi = 1.0$ to 0.8 for cometary impactors (which as noted in Section 3.5.1 may be a more realistic assumption based on N -body simulations) would have resulted in the opposite conclusion for the Earth, i.e. that the atmosphere would grow in cometary impacts and deplete in asteroidal impacts. Similarly, the size distribution plays a strong role, with atmosphere growth favoured more for distributions with the smaller 10 km upper cut-off. This is because impacts with 10–100 km planetesimals destroy atmospheres rather than lead to their growth, so removing these from the distribution increases $\Delta m/m_{ac}$, although only up to a maximum of p_v , which is only reached if all of the accreted planetesimal mass is retained and a negligible fraction of atmosphere lost in impacts (i.e. for low-velocity collisions). Flattening the size distribution (i.e. the thinner lines with $\alpha = 3.0$) has the opposite effect because it then places more of the mass in larger planetesimals.

Clearly, for the Solar system where the size distribution is known for the different impactor populations, and where these populations also have relative velocities that can be derived from N -body simulations, the approach of using a power-law size distribution and single ξ value can inevitably only give an approximation to the outcome of impacts. Instead, the actual distributions should be used, though these still have many uncertainties, particularly when considering the early evolution of the Solar system when the bombardment was greatest (e.g. Morbidelli et al. 2018). Thus, the above discussion should be taken as a caution that the outcome will depend on what is assumed about the relative velocities and

Table 1. Properties of Solar system terrestrial planets, and the predictions of the model for the fractional change in atmosphere mass due to accretion of $3 \times 10^{-5} M_{\oplus}$ of impactors with a size distribution $\alpha = 3.5$ from 1 m up to 100 km of asteroidal ($\rho_{\text{imp}} = 2.8 \text{ g cm}^{-3}$, $p_v = 0.02$, and $\xi = 0.3$) or cometary ($\rho_{\text{imp}} = 0.9 \text{ g cm}^{-3}$ and $\xi = 1$) type.

Planet	a_p	M_p	ρ_p	δ	μ	$(\Delta m_{\text{LHB, ac}}/m)_{\text{ast}}$	$(\Delta m_{\text{LHB, ac}}/m)_{\text{com}}$
Venus	0.72	0.82	5.2	99×10^{-6}	43.5	+0.24 per cent	−1.4 per cent
Earth	1.0	1.0	5.5	0.85×10^{-6}	29.0	+39 per cent	−16 per cent
Mars	1.52	0.11	3.9	0.039×10^{-6}	43.3	−6200 per cent	−24 000 per cent

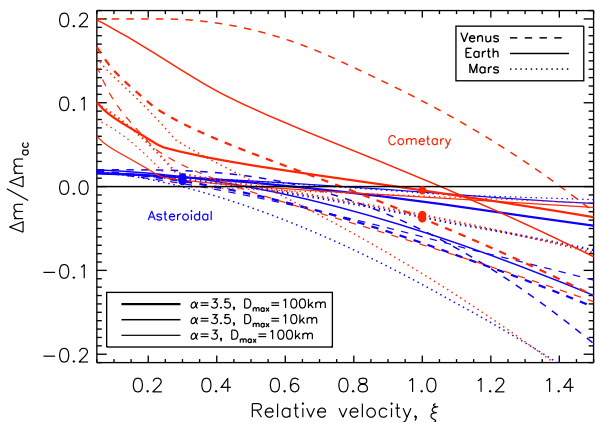


Figure 11. Change in atmosphere mass per accreted impactor mass for the Solar system terrestrial planets assuming their current properties (see Table 1). This is plotted for different assumptions about the impactors with the ratio of the relative velocity of impactors to the planet’s orbital velocity (ξ) on the x-axis. The size distribution is assumed to be a power law from $D_{\text{min}} = 1 \text{ m}$ up to $D_{\text{max}} = 10$ or 100 km , with a slope of $\alpha = 3.0$ or 3.5 . Asteroidal impactors are those with $\rho_{\text{imp}} = 2.8 \text{ g cm}^{-3}$ and $p_v = 0.02$ and cometary impactors are those with $\rho_{\text{imp}} = 0.9 \text{ g cm}^{-3}$ and $p_v = 0.2$. The values for the assumptions used elsewhere in the paper are shown with filled circles.

size distribution (and moreover the prescription for the outcome of collisions) and these all contribute to any differences in conclusions between different authors. For example, de Niem et al. (2012) concluded that both the Earth and Mars atmospheres should grow during the Late Heavy Bombardment, with 300–600 per cent growth for the Earth. Their size distributions are close to a power law with $\alpha = 3$ for the cometary population up to $D_{\text{max}} = 100 \text{ km}$, but are more complex for asteroids (see their fig. 5), while their distributions of impact velocities ξ have means close to 0.5 and 0.8 for asteroids and comets, respectively (see their figs 6 and 7). These still do not explain the different conclusions that must come down to the assumptions about the outcome of impacts, in particular the optimistic assumptions about impactor retention and the role of giant impacts discussed in Section 4.2. Indeed, other authors also find atmospheric loss in impacts (Zahnle 1993; Svetsov 2007; Pham, Karatekin & Dehant 2011; Pham & Karatekin 2016).

While it remains challenging to make accurate predictions for any given planet, the model can still be used to make predictions for trends that may be observable in large samples of planets (see Section 4.5).

4.5 Predictions for exoplanet population

Fig. 12 shows the population of exoplanets discovered by Kepler, then subsequently followed up by the California Kepler Survey to determine their accurate radii (Fulton & Petigura 2018). In the

top left of Fig. 12, the gap in this population, where there is a dearth of transiting exoplanets with radii $\sim 1.5 R_{\oplus}$, is evident. This is interpreted by various authors as evidence of photoevaporation of primordial atmospheres, since it is only those that are sufficiently large that can survive the bombardment of high-energy radiation from the stars shortly after they reach the main sequence (Owen & Wu 2017), although other explanations have been proposed such as the atmospheric mass-loss being caused by the luminosity of the cooling rocky core (Ginzburg et al. 2018).

It is not the purpose of this section to advocate yet another explanation, rather to consider the possible effect of planetesimal bombardment on the atmospheres in this observed exoplanet population, and so to determine whether this may have any consequence for their observable properties. Such consideration faces an obstacle, however, since while the radii and orbital periods of these planets have been measured with high accuracy, and their stellar properties reasonably well constrained, the masses of the planets are unknown. Thus, for this analysis, it will be assumed that the planets have a density of 5.5 g cm^{-3} , and so this addresses the question of how their atmospheres would evolve if they are rocky and their atmospheres contribute little to the observed radius (which has been the assumption throughout this paper), even though this is not thought to be the case for the $\gg 1.5 R_{\oplus}$ planets (Rogers 2015).

For each planet, the model is used to predict the f_v parameter that determines whether the atmosphere will grow or deplete in planetesimal impacts for different assumptions about the atmosphere properties (i.e. its mean molecular weight μ and fractional mass δ) and about the impactor properties (asteroidal or cometary as defined earlier). The different quadrants of the circles shown for each planet are for different combinations of these properties. It is not necessary to focus on the individual quadrants to get the sense that should be clear from the earlier discussion that the atmospheres of planets towards the top right of the plot are more likely to grow in impacts (i.e. have a bluer colour and so $f_v > 1$) while those of planets towards the bottom left of the plot are more likely to deplete in impacts (i.e. have a redder colour and so $f_v < 1$). As discussed previously, the transition between growth and depletion (i.e. the impact shoreline where planets are coloured in white and so have $f_v = 1$) depends on the model assumptions. However, since the most important parameter in the model is the ratio of the planet’s escape velocity to its Keplerian velocity, for each set of assumptions the predicted f_v depends mostly on the combination $R_p^3 t_{\text{per}}$, where t_{per} is the orbital period, as shown in the bottom left of Fig. 12. Fitting a power law for each model shows that $f_v \propto [R_p^3 t_{\text{per}}]^n$, where n is in the range 0.7–1 for the four assumptions shown.

It is noticeable that the planets that are below the gap have atmospheres that are predicted to be depleted in impacts, while those above the gap are predicted to grow secondary atmospheres in impacts. While plotting the observations in this way is not sufficient to extract information about the shape of the gap, for which consideration of the observational biases is required, such a consideration shows that the radius of the planet at which the gap

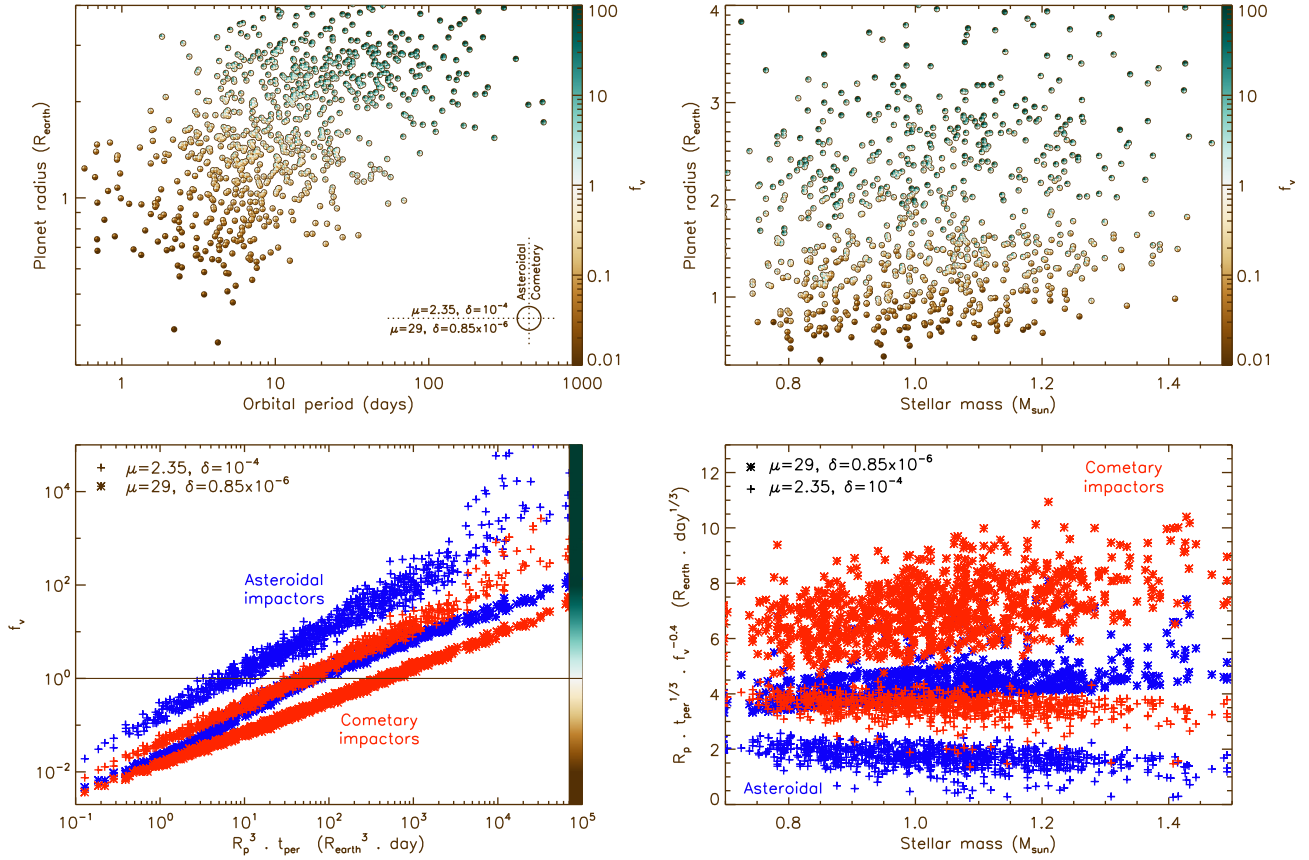


Figure 12. Model predictions for the population of 907 exoplanets from table 4 of Fulton & Petigura (2018). The top two plots show planet radius versus either orbital period (top left) or stellar mass (top right), and so are, respectively, equivalent to figs 4 and 8 of Fulton & Petigura (2018). For each planet, the colour shows the model prediction for f_v as indicated in the colour bar on the right (i.e. blue is $f_v > 1$ meaning the atmosphere grows in impacts; brown is $f_v < 1$ meaning the atmosphere depletes in impacts). The planets are assumed to have a density 5.5 g cm^{-3} , and the predictions are shown for four different further assumptions about the impactors or atmosphere, by dividing each planet’s circle into four quadrants corresponding to the assumptions summarized in the bottom right of the top left plot, i.e. impactors are assumed to be asteroidal ($\rho_{\text{imp}} = 2.8 \text{ g cm}^{-3}$, $p_v = 0.02$) for the left quadrants and cometary ($\rho_{\text{imp}} = 0.9 \text{ g cm}^{-3}$, $p_v = 0.2$) for the right quadrants, and the atmosphere is assumed to be Earth-like ($\delta = 0.85 \times 10^{-6}$, $\mu = 29$) for the bottom quadrants and primordial ($\delta = 10^{-4}$, $\mu = 2.35$) for the top quadrants. The bottom plots show the model predictions for the four different assumptions identified by the colour (blue for asteroidal impactors, and red for cometary impactors) and symbol (asterisk for an Earth-like atmosphere, and plus for primordial atmosphere).

appears decreases with orbital period (Fulton & Petigura 2018; Van Eylen et al. 2018). The same is true for the transition in the model between atmospheres that grow and deplete, i.e. the impact shoreline that from the bottom left plot of Fig. 12 is at a radius that scales $R_p \propto t_{\text{per}}^{-1/3}$. This consideration also shows that the observed gap is at larger planet radius for planets orbiting higher mass stars, which can be seen in the top right of Fig. 12. The trend in the model predictions in this regard is less obvious from the top right panel, so this is considered further in the bottom right panel in which the general trend of the bottom left panel has been removed by assuming $n = 0.84$ and so plotting $R_p \cdot t_{\text{per}}^{1/3} \cdot f_v^{-0.4}$ against stellar mass. This allows us to seek for an additional stellar mass dependence (i.e. in addition to that arising through the orbital period) of the form $f_v \propto [R_p^3 \cdot t_{\text{per}}]^n M_\star^\gamma$, since the plotted value would be $\propto M_\star^{-\gamma/(3n)}$ and so flat for $\gamma = 0$. The plotted value can also be used to assess the planet radius at which the $f_v = 1$ transition would occur for a fixed orbital period, and shows that for models with Earth-like atmospheres this would appear at larger planetary radii for higher mass stars (like the trend for the observed gap). However, the opposite is true for models with more massive primordial atmospheres.

While the model trends show some similarities to the observed properties of the gap, it should be cautioned that this does not mean that planetesimal bombardment would reproduce the observations (e.g. Lopez & Rice 2018). For example, this application pushes the model into a regime where its assumption that the atmospheres are low in mass breaks down, and any observable consequence on the properties of the population may require an unrealistic level of planetesimal bombardment. The most secure way of interpreting the model predictions in Fig. 12 is to consider the effect of bombardment on a planet that is born with a low-mass (e.g. Earth-like) atmosphere. The prediction is that planets below the gap would find it hard to grow a secondary atmosphere due to impacts. However, since more massive atmospheres have a larger f_v , if they do start to grow an atmosphere then this likely becomes easier, but this does not address the question of whether the planet can grow an atmosphere that is massive enough to become inflated and so change its position on the plot and so be responsible for the gap. That would depend on the amount accreted and on how the physics changes as the atmosphere becomes more massive, for example the higher mean molecular weight of a secondary atmosphere could mean that a significantly higher fraction of the planet’s mass than a few per cent

is required to be accreted for it to appear inflated (e.g. by a factor of $\sim \mu_{\oplus}/\mu_{\odot} \approx 12$). But if the current model were applicable to more massive atmospheres, its predictions for atmosphere growth of $\Delta m/m_{ac}$ of a few per cent (see Fig. 5) would suggest that bombardment levels comparable with the planet mass are required to attain an atmosphere of a few per cent.

The prediction that planets below the gap cannot grow secondary atmospheres by impacts also applies to planets that may have lost their atmosphere due to photoevaporation, since that may be the origin of the gap and bombardment may continue after that process is complete. Thus, it is worth noting that the prediction is to some extent dependent on the assumptions about the impacts, so that planets just below the gap may be able to grow secondary atmospheres if the impact conditions are right (i.e. some of the planets below the gap have quadrants that are light blue in Fig. 12). Depending on the exact slope of the gap, it could be that planets at larger distance from the star are more amenable to growth of impact-generated secondary atmospheres (following loss of their primordial atmospheres by photoevaporation).

The interpretation of the predictions for the effect of bombardment on a planet that is born with a massive atmosphere is less secure. However, this shows that for planets below the gap such atmospheres would be expected to be depleted, though of course only if sufficient bombardment occurs. As above, if the current model were applicable to more massive atmospheres, its prediction for atmosphere loss of $\Delta m/m_{ac}$ of the order of 1 per cent (see Fig. 5) would suggest that bombardment levels comparable with the planet mass would be required to remove a few per cent atmosphere. For planets above the gap, their atmospheres would be expected to grow in impacts, and to become more volatile rich. If future observations show their atmospheres to be volatile rich, then this model would support planetesimal impacts being one possible origin for the volatiles. It must, however, be noted that volatile-rich atmospheres may also be replenished by outgassing (as may be the case for Mars, for example, Craddock & Greeley 2009), a process that is not considered here.

4.6 Implications for life

With the origin of life on the Earth still debated, uncertainty in extrapolating to other planetary systems is unavoidable. However, impacts are often considered to play a positive role, for example by delivery of organic molecules or their synthesis in impact shocks (Chyba & Sagan 1992; Patel et al. 2015), or by the delivery of water to otherwise dry planets (e.g. Chyba 1990). Though impacts may also inhibit the further development of life (Maher & Stevenson 1988). Since the Earth's evolution was evidently conducive to the development of life, then if we make the anthropocentric assumption that a similar evolution in terms of a planet's atmosphere might be similarly conducive to life, the results from this paper can be used to make relative statements about whether planets in the habitable zones of other stars would be more or less conducive to the development of life.

Fig. 13 shows the change in atmosphere mass for an Earth-like planet in the habitable zone of stars of different luminosities. Here, it has been assumed that $L_{\star} = M_{\star}^3$ (for units of L_{\odot} and M_{\odot}), and the habitable zone is simply taken as the distance at which its temperature is 278 K so that $a_p = \sqrt{L_{\star}}$ (see e.g. Kopparapu et al. 2014, for a more detailed definition). It then considers the fractional change in the atmosphere for different assumptions about the impacting planetesimals. This shows that there is a general tendency for habitable planets around lower luminosity stars to be

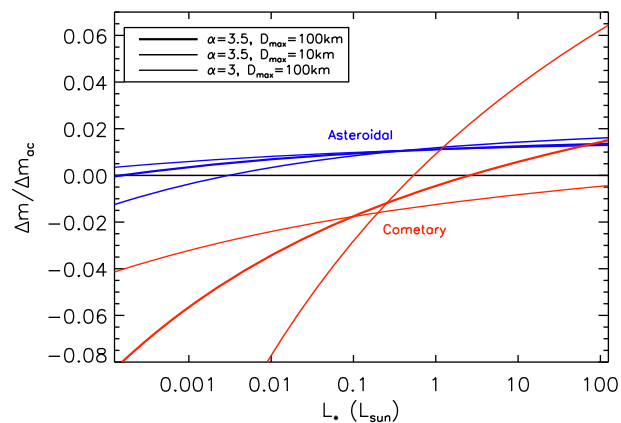


Figure 13. Change in atmosphere mass per accreted impactor mass for Earth-like planets ($1 M_{\oplus}$ with a $0.85 \times 10^{-6} M_{\oplus}$ atmosphere with $\mu = 29$) in the habitable zone of stars of different luminosities (i.e. $a_p = \sqrt{L_{\star}}$, assuming $M_{\star} \propto L_{\star}^{1/3}$). This is plotted for different assumptions about the impactors. The size distribution is assumed to be a power law from $D_{\min} = 1$ m up to $D_{\max} = 10$ or 100 km, with a slope of $\alpha = 3.0$ or 3.5 . Asteroidal impactors are those with $\rho_{\text{imp}} = 2.8 \text{ g cm}^{-3}$, $p_v = 0.02$, and $\xi = 0.3$, and cometary impactors are those with $\rho_{\text{imp}} = 0.9 \text{ g cm}^{-3}$, $p_v = 0.2$, and $\xi = 1.0$.

more susceptible to having their atmospheres depleted in collisions, which is true regardless of the assumption about the impacting planetesimals. This is because the habitable zone is closer in for lower luminosity stars, which, even when accounting for the slower orbital velocity due to the lower stellar mass, results in higher collision velocities and so more destructive impacts (for the given assumptions, the collision velocity in the habitable zone scales $\propto M_{\star}^{-1/4}$).

There is already much discussion about the habitability of planets around low-mass M stars (e.g. Shields, Ballard & Johnson 2016), since close-in planetary systems are common around such stars, and the proximity of the habitable zone to low-luminosity stars makes these planets relatively easy to detect and further characterize using transit observations (e.g. de Wit et al. 2018). However, it was shown that such planets that end up in the habitable zone would have exceeded the runaway greenhouse threshold on the pre-main sequence and so would have lost any water (Ramirez & Kaltenegger 2014), which is confounded by issues such as the high incidence of flares on low-mass stars that would be detrimental to habitability (Vida et al. 2017; Tilley et al. 2019), and the likelihood of these habitable zone planets to be tidally locked to the host star with consequences for atmospheric dynamics (Kopparapu et al. 2016). Impacts could provide a potential solution to some of these issues, by delivering a secondary atmosphere and water to the planets. However, Fig. 13 shows that, at least as long as the impacting planetesimals have similar properties to those hitting the Earth, impacts are more likely to destroy the atmosphere of a habitable zone planet around a low-mass star than to replenish it. Fortunately, the impacting planetesimals may have a different impact velocity distribution, so that habitable zone planets could still grow substantial atmospheres as was found for the TRAPPIST-1 planets by Kral et al. (2018).

In any case, it might be noted that planets in the habitable zones of higher mass stars may be more susceptible to the growth of a secondary atmosphere in impacts. Although the fact that the lines are relatively flat in Fig. 13 (at least for certain assumptions) could also be taken to infer that the atmospheres of Earth-like

habitable zone planets do not suffer significantly different fates to the Earth as a result of impacts. However, a strong conclusion on this would require knowledge of the possible impacting planetesimal population, which may be systematically different around stars of different spectral types. There is also the caveat that water could be retained in the magma ocean during formation and outgassed later on (Peslier et al. 2017; Ikoma et al. 2018), so that an Earth-like impact history may not be a necessary requirement for the development of life.

5 CONCLUSION

This paper has developed a model for the evolution of planetary atmospheres due to planetesimal impacts that accounts for both stripping of the atmosphere and the delivery of volatiles. It is based on a suite of simulations of impacts that covers a wide range of planetary atmosphere and impacting planetesimal properties. The implications of the model for the atmosphere evolution of planets in different regions of parameter space are discussed, and the relative simplicity of the parametrization means that it is possible to understand both qualitatively and quantitatively the dependence of the outcome on the different input parameters (i.e. the impacting planetesimals' densities, volatile fractions, and impact velocities, as well as the planet mass, orbital distance and atmospheric mass and composition, and the stellar properties).

The conclusion is that planets are divided in planet mass versus semimajor axis parameter space into those with atmospheres that deplete in impacts (if they are close to the star and/or low in mass) and those that can grow secondary volatile-rich atmospheres (if they are far from the star and/or high in mass). The dividing line, or impact shoreline, is parallel to one of constant ratio of orbital velocity to escape velocity, and is analogous to the cosmic shoreline discussed in Zahnle & Catling (2017) that was interpreted as a consequence of irradiation. The location of the impact shoreline depends on assumptions about impacting planetesimals, and for different (reasonable) assumptions there is more than an order of magnitude spread, say in terms of its location in planet mass for a given orbital distance. For Sun-like stars, a planet with properties like the Earth would sit near the shoreline.

Impact-driven atmosphere evolution is dominated by the combined effect of accreting 1–20 km planetesimals, so as long as the size distribution extends beyond this range, the conclusions are largely independent of the size distribution. However, the model presented herein is based on simulations appropriate for low-mass atmospheres, and further development is needed to consider the situation for massive atmospheres for which such planetesimals would undergo an aerial burst (rather than be destroyed on reaching the planet surface). As in previous studies, giant impacts are found to have little effect on atmosphere evolution unless the atmosphere is a significant fraction of the planet mass, though they may introduce an element of stochasticity when impactors are comparable in mass to the planet.

Applying the model to the Solar system terrestrial planets shows that whether the Earth's atmosphere grows or depletes in impacts is strongly dependent on the distribution of impact velocities and impactor properties. Further discussion of this is deferred to a later paper where these distributions can be considered in more detail.

Application to the population of transiting exoplanets discovered by Kepler shows that the gap in the planet radius distribution is roughly coincident with the dividing line (impact shoreline) between planets with atmospheres that grow and deplete in collisions. The dependence of this dividing line on orbital distance and

stellar mass is also similar to that observed. It seems unlikely that bombardment levels would have been sufficient to be responsible for the gap, either by depleting the primordial atmospheres of the smallest planets, or by growing substantial secondary atmospheres for the most massive planets, since this would require bombardment by a mass comparable to the planets (and even such high bombardment levels may not be sufficient). However, it must be remembered that the predictions of the model are inaccurate for planets with atmospheres as massive as those inferred for planets above the gap (i.e. a few per cent of the planet mass). Nevertheless, this coincidence shows that the effect of impacts on planetary atmospheres deserves further consideration. It is also possible to draw firmer conclusions about planets below the gap, for example, that if these atmospheres were depleted by stellar irradiation, then they would be unlikely to grow a secondary atmosphere in impacts, except for those just below the gap and for certain conditions on the impacting planetesimals. Consideration of planets in the habitable zone of stars of different masses shows that impacts are more harmful for those of lower mass stars (see also Kral et al. 2018). Thus, if an Earth-like bombardment, and its effect on the Earth's atmosphere, was a requirement for the development of life, this may give cause to disfavour M stars as the hosts of life-bearing planets. However, without consideration of the impactor populations, or of the other factors relevant to the evolution of the conditions on the planetary surface, this cannot be a strong conclusion.

REFERENCES

- Ahrens T. J., 1993, *Annu. Rev. Earth Planet. Sci.*, 21, 525
 Biersteker J. B., Schlichting H. E., 2019, *MNRAS*, 485, 4454
 Brouwers M. G., Vazan A., Ormel C. W., 2018, *A&A*, 611, A65
 Cameron A. G. W., 1983, *Icarus*, 56, 195
 Cataldi G., Brandeker A., Thébaud P., Singer K., Ahmed E., de Vries B. L., Neubeck A., Olofsson G., 2017, *Astrobiology*, 17, 721
 Charbonneau D., Brown T. M., Noyes R. W., Gilliland R. L., 2002, *ApJ*, 568, 377
 Chyba C. F., 1990, *Nature*, 343, 129
 Chyba C., Sagan C., 1992, *Nature*, 355, 125
 Chyba C. F., Thomas P. J., Brookshaw L., Sagan C., 1990, *Science*, 249, 366
 Craddock R. A., Greeley R., 2009, *Icarus*, 204, 512
 Dauphas N., 2003, *Icarus*, 165, 326
 Defrère D. et al., 2018, *Exp. Astron.*, 46, 543
 de Niem D., Kührt E., Morbidelli A., Mutschmann U., 2012, *Icarus*, 221, 495
 de Wit J. et al., 2018, *Nat. Astron.*, 2, 214
 Dohnanyi J. S., 1969, *J. Geophys. Res.*, 74, 2531
 Elkins-Tanton L. T., 2012, *Annu. Rev. Earth Planet. Sci.*, 40, 113
 Elkins-Tanton L. T., Seager S., 2008, *ApJ*, 685, 1237
 Fulton B. J., Petigura E. A., 2018, *AJ*, 156, 264
 Fulton B. J. et al., 2017, *AJ*, 154, 109
 Genda H., Abe Y., 2003, *Icarus*, 164, 149
 Genda H., Abe Y., 2005, *Nature*, 433, 842
 Gillmann C., Golabek G. J., Tackley P. J., 2016, *Icarus*, 268, 295
 Gillon M. et al., 2017, *Nature*, 542, 456
 Ginzburg S., Schlichting H. E., Sari R., 2018, *MNRAS*, 476, 759
 Godolt M., Tosi N., Stracke B., Grenfell J. L., Ruedas T., Spohn T., Rauer H., 2019, *A&A*, 625, A12
 Gomes R., Levison H. F., Tsiganis K., Morbidelli A., 2005, *Nature*, 435, 466
 Grady M. M., Wright I. P., 2003, *Space Sci. Rev.*, 106, 231
 Griffith C. A., Zahnle K., 1995, *J. Geophys. Res.*, 100, 16907
 Huang C. X. et al., 2018, *ApJ*, 868, L39
 Ikoma M., Elkins-Tanton L., Hamano K., Suckale J., 2018, *Space Sci. Rev.*, 214, 76

- Jackson A. P., Davis T. A., Wheatley P. J., 2012, *MNRAS*, 422, 2024
- Jin S., Mordasini C., 2018, *ApJ*, 853, 163
- Kaltenegger L., 2017, *ARA&A*, 55, 433
- Kasting J. F., Catling D., 2003, *ARA&A*, 41, 429
- Kopparapu R. K., Ramirez R. M., SchottelKotte J., Kasting J. F., Domagal-Goldman S., Eymet V., 2014, *ApJ*, 787, L29
- Kopparapu R. K., Wolf E. T., Haq-Misra J., Yang J., Kasting J. F., Meadows V., Terrien R., Mahadevan S., 2016, *ApJ*, 819, 84
- Kral Q., Wyatt M. C., Triaud A. H. M. J., Marino S., Thébault P., Shorttle O., 2018, *MNRAS*, 479, 2649
- Lammer H. et al., 2014, *MNRAS*, 439, 3225
- Lammer H. et al., 2018, *A&AR*, 26, 2
- Lecavelier Des Etangs A., 2007, *A&A*, 461, 1185
- Lehmer O. R., Catling D. C., 2017, *ApJ*, 845, 130
- Levison H. F., Duncan M. J., 1997, *Icarus*, 127, 13
- Lopez E. D., Fortney J. J., 2014, *ApJ*, 792, 1
- Lopez E. D., Rice K., 2018, *MNRAS*, 479, 5303
- Lozovsky M., Helled R., Dorn C., Venturini J., 2018, *ApJ*, 866, 49
- Maher K. A., Stevenson D. J., 1988, *Nature*, 331, 612
- Marino S., Bonsor A., Wyatt M. C., Kral Q., 2018, *MNRAS*, 479, 1651
- Marty B. et al., 2016, *Earth Planet. Sci. Lett.*, 441, 91
- Marty B. et al., 2017, *Science*, 356, 1069
- Melosh H. J., 1989, *Impact Cratering: A Geologic Process*. Oxford University Press; Oxford: Clarendon Press, New York
- Melosh H. J., Vickery A. M., 1989, *Nature*, 338, 487
- Morbideilli A., Nesvornyy D., Laurenz V., Marchi S., Rubie D. C., Elkins-Tanton L., Wicczorek M., Jacobson S., 2018, *Icarus*, 305, 262
- Mumma M. J., Charnley S. B., 2011, *ARA&A*, 49, 471
- O’Keefe J. D., Ahrens T. J., 1989, *Nature*, 338, 247
- Owen T., Bar-Nun A., 1995, *Icarus*, 116, 215
- Owen J. E., Wu Y., 2017, *ApJ*, 847, 29
- Patel B. H., Percivalle C., Ritson D. J., Duffy C. D., Sutherland J. D., 2015, *Nat. Chem.*, 7, 301
- Peslier A. H., Schönbächler M., Busemann H., Karato S.-I., 2017, *Space Sci. Rev.*, 212, 743
- Pham L. B. S., Karatekin Ö., 2016, *Planet. Space Sci.*, 125, 1
- Pham L. B. S., Karatekin Ö., Dehant V., 2011, *Planet. Space Sci.*, 59, 1087
- Pollack J. B., Hubickyj O., Bodenheimer P., Lissauer J. J., Podolak M., Greenzweig Y., 1996, *Icarus*, 124, 62
- Pope K. O., Baines K. H., Ocampo A. C., Ivanov B. A., 1997, *J. Geophys. Res.*, 102, 21645
- Prinn R. G., Fegley B., 1987, *Annu. Rev. Earth Planet. Sci.*, 15, 171
- Ramirez R. M., Kaltenegger L., 2014, *ApJ*, 797, L25
- Rauer H. et al., 2014, *Exp. Astron.*, 38, 249
- Rogers L. A., 2015, *ApJ*, 801, 41
- Rubin M. et al., 2019, *MNRAS*, 489, 594
- Schaefer L., Fegley B., 2010, *Icarus*, 208, 438
- Schlichting H. E., Mukhopadhyay S., 2018, *Space Sci. Rev.*, 214, 34
- Schlichting H. E., Sari R., Yalinewich A., 2015, *Icarus*, 247, 81
- Schneider J., Dedieu C., Le Sidaner P., Savalle R., Zolotukhin I., 2011, *A&A*, 532, A79
- Sephton M. A., 2002, *Nat. Prod. Rep.*, 19, 292
- Shields A. L., Ballard S., Johnson J. A., 2016, *Phys. Rep.*, 663, 1
- Shuvalov V., 2009, *Meteorit. Planet. Sci.*, 44, 1095
- Shuvalov V., Kürt E., de Niem D., Wünnemann K., 2014, *Planet. Space Sci.*, 98, 120
- Svetsov V. V., 2007, *Sol. Syst. Res.*, 41, 28
- Tilley M. A., Segura A., Meadows V., Hawley S., Davenport J., 2019, *Astrobiology*, 19, 64
- Van Eylen V., Agentoft C., Lundkvist M. S., Kjeldsen H., Owen J. E., Fulton B. J., Petigura E., Snellen I., 2018, *MNRAS*, 479, 4786
- Vickery A. M., Melosh J. J., 1990, in Sharpton V. L., Ward P. D., eds, *Global Catastrophes in Earth History; An Interdisciplinary Conference on Impacts, Volcanism, and Mass Mortality: Geological Society of America Special Paper 247*, Geological Society of America. p. 289
- Vida K., Kővári Z., Pál A., Oláh K., Kriskovics L., 2017, *ApJ*, 841, 124
- Vidal-Madjar A., Lecavelier des Etangs A., Désert J.-M., Ballester G. E., Ferlet R., Hébrard G., Mayor M., 2003, *Nature*, 422, 143
- Walker J. C. G., Hays P. B., Kasting J. F., 1981, *J. Geophys. Res.*, 86, 9776
- Wetherill G. W., Stewart G. R., 1993, *Icarus*, 106, 190
- Wolfgang A., Lopez E., 2015, *ApJ*, 806, 183
- Wyatt M. C., Clarke C. J., Booth M., 2011, *Celest. Mech. Dyn. Astron.*, 111, 1
- Wyatt M. C., Farihi J., Pringle J. E., Bonsor A., 2014, *MNRAS*, 439, 3371
- Wyatt M. C., Bonsor A., Jackson A. P., Marino S., Shannon A., 2017, *MNRAS*, 464, 3385
- Zahnle K. J., 1993, *J. Geophys. Res.*, 98, 10
- Zahnle K. J., Catling D. C., 2017, *ApJ*, 843, 122
- Zahnle K., Pollack J. B., Grinspoon D., Dones L., 1992, *Icarus*, 95, 1
- Zahnle K., Arndt N., Cockell C., Halliday A., Nisbet E., Selsis F., Sleep N. H., 2007, *Space Sci. Rev.*, 129, 35
- Zahnle K. J., Gacesa M., Catling D. C., 2019, *Geochim. Cosmochim. Acta*, 244, 56
- Zeng L., Sasselov D. D., Jacobsen S. B., 2016, *ApJ*, 819, 127
- Zhu M.-H., Artemieva N., Morbidelli A., Yin Q.-Z., Becker H., Wünnemann K., 2019, *Nature*, 571, 226

APPENDIX A: PARAMETER SUMMARY

Table A1. Summary of parameters used in the paper and their units.

Parameter	Units	Meaning
a_p	au	Planet semimajor axis
D	m	Impactor diameter
D_{GI}	m	Impactor diameter above which giant impacts dominate atmosphere mass-loss
D_{min}	m	Minimum impactor diameter
D_{max}	m	Maximum impactor diameter
f_v	–	Ratio of gain of atmosphere mass due to impactor retention to mass-loss in impacts
H	m	Atmospheric scale height
L_*	L_\odot	Stellar luminosity
M_*	M_\odot	Stellar mass
M_p	M_\oplus	Planet mass
m	M_\oplus	Total atmosphere mass
\dot{m}^-	$M_\oplus \text{ s}^{-1}$	Atmospheric mass-loss rate
\dot{m}_v^+	$M_\oplus \text{ s}^{-1}$	Rate at which atmosphere gains volatiles due to impactor retention
m_{inc}	M_\oplus	Total mass of impactors put on planet crossing orbits
m_{ac}	M_\oplus	Total mass of impactors accreted by the planet
$m_{atmloss}(D)$	M_\oplus	Atmospheric mass lost in impact with impactor of diameter D
$m_{impacc}(D)$	M_\oplus	Mass of impactor of diameter D that is retained by planet
$m_{atmloss}$	M_\oplus	Atmospheric mass lost integrated over the impactor size distribution
$m_{atmlss, GI}$	M_\oplus	Atmospheric mass lost by giant impacts integrated over the impactor size distribution
m_{impacc}	M_\oplus	Impactor mass retained by planet integrated over the impactor size distribution
m_0	M_\oplus	Total initial atmosphere mass
m_p	M_\oplus	Mass of primordial component of atmosphere
m_v	M_\oplus	Mass of volatile (secondary) component of atmosphere
m_{imp}	M_\oplus	Mass of impacting planetesimal
$n(D)dD$	–	The number of impactors in a size range from D to $D + dD$
p_v	–	Fraction of retained impactor mass that goes into the atmosphere
q	au	Pericentre distance of impactor orbit
R_{ac}	s^{-1}	Rate at which impactors collide with the planet
R_{ej}	s^{-1}	Rate at which impactors are ejected by the planet
R_{dyn}	s^{-1}	Rate at which impactors are removed dynamically from planet-crossing orbits
R_p	m	Planet radius
T	K	Temperature of planet atmosphere
t	s	Time
t_0	s	Time for atmosphere to deplete in absence of volatile replenishment, $t_0 = m_0/\dot{m}_0^-$
t_{bare}	s	Time for atmosphere to be completely depleted
t_{per}	day	Orbital period
v_{imp}	m s^{-1}	Impact velocity
v_p	m s^{-1}	Planet's orbital velocity
v_{esc}	m s^{-1}	Planet's escape velocity
x	–	Parameter equal to $(m_{imp}/M_p)(v_{imp}/v_{esc})$
α	–	Power-law index of impactor size distribution
δ	–	Ratio of atmosphere mass to planet mass
δ_0	–	Ratio of initial atmosphere mass to planet mass
δ_{GI}	–	Ratio of atmosphere to planet mass above which giant impacts dominate evolution
η	–	Parameter that for a given planet and scenario scales with impactor size cubed
η_{ab}	–	Defines the smallest planetesimal that does not undergo aerial burst before impact
η_{maxret}	–	Defines the largest impacting planetesimal whose mass can be retained by the planet
η_{tr}	–	Defines the smallest planetesimal that does not fragment in atmosphere before impact
μ	–	Mean molecular weight of atmosphere
ξ	–	Averaged ratio of planet–impactor relative velocity to planet orbital velocity
ρ_0	g cm^{-3}	Atmosphere density at surface
ρ_p	g cm^{-3}	Planet density
ρ_{ps}	g cm^{-3}	Density of the planetary surface
ρ_{imp}	g cm^{-3}	Impactor density
χ_a	–	Parameter used to determine atmospheric mass-loss in collision
χ_{pr}	–	Parameter used to determine impactor retention in collision

This paper has been typeset from a $\text{\TeX}/\text{\LaTeX}$ file prepared by the author.